

# Quantifying vegetation biophysical variables from imaging spectroscopy data: a review on retrieval methods

Jochem Verrelst<sup>1</sup>, Zbyněk Malenovský<sup>2,3,4</sup>, Christiaan Van der Tol<sup>5</sup>, Gustau Camps-Valls<sup>1</sup>, Jean-Philippe Gastellu-Etchegorry<sup>6</sup>, Philip Lewis<sup>7</sup>, Peter North<sup>8</sup>, and Jose Moreno<sup>1</sup>

<sup>1</sup>Image Processing Laboratory, Universitat de València, Spain.

<sup>2</sup>Surveying and Spatial Sciences Group, School of Technology, Environments and Design, University of Tasmania, Private Bag 76, TAS 7001 Hobart, Australia

<sup>3</sup>Global Change Research Institute CAS, Remote Sensing Department,

Bělidla 986/4a, 603 00 Brno, Czech Republic

<sup>4</sup>USRA/GESTAR, NASA Goddard Space Flight Center, Biospheric Sciences Laboratory, 8800 Greenbelt Rd, Greenbelt, MD 20771, USA

<sup>5</sup>Department of Water Resources, Faculty ITC, University of Twente, P.O. Box 217, 7500 AE Enschede, The Netherlands

<sup>6</sup>Centre d'Etudes Spatiales de la Biosphère - UPS, CNES, CNRS, IRD, Université de Toulouse, 31401 Toulouse Cedex 9, France

<sup>7</sup>Department of Geography, University College London, Pearson Building, Gower Street, London WC1E 6BT, UK

<sup>8</sup>Department of Geography, Swansea University, SA2 8PP Swansea, UK

**Abstract** An unprecedented spectroscopic data stream will soon become available with forthcoming Earth-observing satellite missions equipped with imaging spectroradiometers. This data stream will open up a vast array of opportunities to quantify a diversity of biochemical and structural vegetation properties. The processing requirements for such large data streams require reliable retrieval techniques enabling the spatio-temporally explicit quantification of biophysical variables. With the aim of preparing for this new era of Earth observation, this review summarizes the state-of-the-art retrieval methods that have been applied in experimental imaging spectroscopy studies inferring all kinds of vegetation biophysical variables. Identified retrieval methods are categorized into: (1) parametric regression, including vegetation indices, shape indices and spectral transformations; (2) non-parametric regression, including linear and non-linear machine learning regression algorithms; (3) physically-based, including inversion of radiative transfer models (RTMs) using numerical optimization and look-up table approaches; and (4) hybrid regression methods, which combine RTM simulations with machine learning regression methods. For each of these categories, an overview of widely applied methods with application to mapping vegetation properties is given. In view of processing imaging spectroscopy data, a critical aspect involves the challenge of dealing with spectral multicollinearity. The ability to provide robust estimates, retrieval uncertainties and acceptable retrieval processing speed are other important aspects in view of operational processing. Recommendations towards new-generation spectroscopy-based processing chains for operational production of biophysical variables are given.

## 1 Introduction

Quantitative vegetation variable extraction is fundamental to assess the dynamic response of vegetation to changing environmental conditions. Earth observation sensors in the optical domain enable the spatiotemporally-explicit retrieval of plant biophysical variables. This data stream has never been so rich as is foreseen with the new generation imaging spectrometer missions. The forthcoming EnMAP (Guanter et al, 2015), HypIRI (Lee et al, 2015), PRISMA (Labate et al, 2009) and FLEX (Drusch et al, 2017) satellite missions will produce large spectroscopic data streams for land monitoring, which will soon become available to a diverse user community. This upcoming vast data stream will not only be standardized (e.g. atmospherically-corrected), but will also require reliable and efficient retrieval processing techniques that are accurate, robust and fast.

Since the advent of optical remote sensing science, a variety of retrieval methods for vegetation attribute extraction emerged. Most of these methods have been applied to the data of traditional multispectral sensors (Verrelst et al, 2015), but increasingly they are also applied within imaging spectroscopy studies. This review provides a summary of recently developed methodologies to infer per-pixel biophysical variables from imaging spectroscopy data, covering the visible, near-infrared (NIR) and shortwave infrared spectral regions. Essentially, quantification of surface biophysical variables from spectral data always relies on a model, enabling the interpretation of spectral observations and their translation into a surface biophysical variable. Biophysical variable retrievals, as traditionally described in terrestrial remote sensing literature, are grouped into two categories: (1) the statistical (or variable-driven) category; and (2) the physical (or radiometric data-driven) category (Baret and Buis, 2008). Over the last decade, however, both methodological categories expanded into sub-categories and combinations thereof. Exemplary is the increasing number of elements of both categories which have been integrated into *hybrid* approaches. This methodological expansion, therefore, demands for a more systematic categorization. From an optical remote sensing point of view, and in line with an earlier, more general review paper (Verrelst et al, 2015), retrieval methods can be classified in the following four methodological categories:

1. *Parametric regression methods*: Parametric methods assume an explicit relationship between spectral observations and a specific biophysical variable. Thus, explicit parameterized expressions are built usually based on some physical knowledge of absorption and scattering properties and statistical relationship between the variable and the spectral response. Typically a band arithmetic formulation is defined (e.g., a spectral index) and then linked to the variable of interest based on a fitting function.
2. *Non-parametric regression methods*: Non-parametric methods directly define regression functions according to information from the given spectral data and associated variable, i.e., they are data-driven methods. Hence, in contrast to parametric regression methods, a non-explicit choice is to be made on spectral band relationships, transformation(s) or fitting function. Non-parametric methods can further be split into linear or nonlinear regression methods.
3. *Physically-based model inversion methods*: Physically-based algorithms are applications of physical laws establishing photon interaction cause-effect relationships. Model variables are inferred based on specific knowledge, typically obtained with radiative transfer functions.
4. *Hybrid regression methods*: A hybrid-method combines elements of non-parametric statistics and physically-based methods. Hybrid models rely on the generic properties of physically-based methods combined with the flexibility and computational efficiency of non-parametric nonlinear regression methods.

90 These categories provide a theoretical framework to organize the myriad of retrieval meth-  
91 ods, as well to overview the diversity of published imaging spectroscopy applications based  
92 on these methods. However, a few remarks must be considered. One should be aware that  
93 the boundaries of these categories are not always clearly defined; for instance, spectral in-  
94 dices are also often used as input into non-parametric methods. Another important aspect is  
95 that the majority of the here reviewed methods is not exclusively designed for retrieval of  
96 biophysical variables. This especially holds for the statistical methods, whereby a regression  
97 model is used to link spectral data with a biophysical variable. In optical remote sensing sci-  
98 ence these methods are commonly applied to map any feasible continuous variable, as well  
99 in the domains of snow, water or soil properties (see [Matthews \(2011\)](#), [Mulder et al \(2011\)](#)  
100 and [Dietz et al \(2012\)](#) for reviews). Nevertheless, to keep this review comprehensive, it is  
101 limited to retrieval methods with applications in the domain of vegetation properties map-  
102 ping. On the other hand, even within these boundaries each of the above methodological cat-  
103 egories continue to be expanded with all kinds of spectroscopic data processing applications  
104 (e.g. [Gewali et al, 2018](#)). The drivers behind this methodological expansion can be found  
105 in the: (1) interminable increase of computational power, (2) the increasing availability and  
106 democratizing of spectroscopic data, and (3) the steady progress in imaging spectroscopy  
107 sensor technology, which produces each time more sensitive sensors. This progress in imag-  
108 ing spectroscopy technology enables to infer each time more subtle and highly dynamic  
109 vegetation properties from spectral data. For instance, the forthcoming FLEX mission aims  
110 to deliver a portfolio of dynamic plant stress and productivity variables based on, among  
111 others, the exploitation of sun-induced chlorophyll fluorescence emitted by terrestrial vege-  
112 tation ([Drusch et al, 2017](#)). Hence, this underlines the fact that the list of biophysical vari-  
113 ables that can be extracted from imaging spectroscopy is not closed, but instead continues  
114 to grow with ongoing progress in spectrometer technology. Consequently, biophysical vari-  
115 ables are in this review paper defined as any vegetation property that can be quantified,  
116 i.e. any pigments, chemical constituents, structural variables, but also variables related to  
117 plant photosynthesis, productivity or diseases. Altogether, the drivers behind methodolog-  
118 ical expansion are not mutually exclusive, but they strengthen each other, which leads to  
119 a rapid progress in the development of advanced retrieval methods that goes hand in hand  
120 with improved capabilities to quantify a broad diversity of biophysical variables. As will be  
121 demonstrated throughout this review, these trends are resulting in an unprecedented richness  
122 of imaging spectroscopy mapping applications.

123 Regardless of the used methodology or the targeted application, the principal characteristic  
124 of spectroscopic data lies in their dense information content embedded in a few hundred  
125 spectrally narrow bands. Although such spectrally dense data source proved to be beneficial  
126 for the majority of targeted mapping applications, a key challenge for many retrieval meth-  
127 ods is how to deal with spectral multicollinearity, i.e. band redundancy. Special attention,  
128 therefore, will be devoted to address common spectroscopic data processing challenges, and  
129 solutions will be given how to overcome them. Finally, while imaging spectrometers are so  
130 far mostly applied in an experimental context, the developments towards operational systems  
131 have manifestly taken off – and undoubtedly will lead to new directions and possibilities of  
132 Earth observation. In view of [getting prepared for these upcoming](#) global spectroscopic data  
133 streams, we will close this review with recommendations about the possibilities of integrat-  
134 ing promising retrieval approaches into operational schemes.

## 135 2 Parametric regression methods

136 Parametric regression methods have long been the most popular method to quantify bio-  
 137 physical variables in optical remote sensing; and the field of imaging spectroscopy is no  
 138 exception to that. This simplest way of developing a regression model explicitly determines  
 139 parameterized expressions relating a limited number of spectral bands with a biophysical  
 140 variable of interest. The empirical models rely on a selection of bands with high sensitivi-  
 141 ty towards the variable of interest, typically in combination with subtle spectral features to  
 142 reduce undesired effects; related to variations of, for instance, other leaf or canopy prop-  
 143 erties, background soil reflectance, solar illumination and sensor viewing geometry and  
 144 atmospheric composition (e.g. Verrelst et al, 2008, 2010). In the following overview we  
 145 present common parametric regression methods, which are based on (1) vegetation indices,  
 146 (2) shape indices, and (3) spectral transformations.

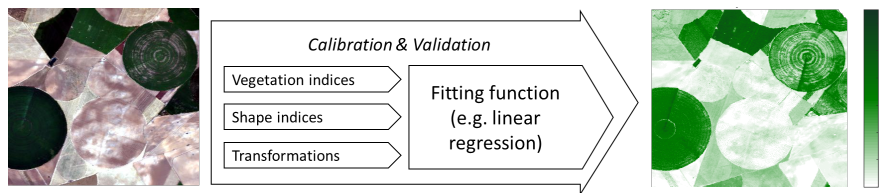


**Fig. 1** Principles of parametric regression. Left: RGB subset of a hyperspectral HyMap image (125 bands) over Barrax agricultural site (Spain). Right: illustrative map of a vegetation property (LAI,  $\text{m}^2/\text{m}^2$ ) as obtained by a 2-band normalized difference index and linear regression. The model was validated with a  $R^2$  of 0.89 (RMSE: 0.63; NRMSE 10.1%). It took 0.2 seconds to produce the map using ARTMO's SI toolbox (Rivera et al, 2014). No uncertainty estimates are provided.

### 147 2.1 Discrete spectral band approaches: vegetation indices

148 Parametric regression models based on vegetation indices (VIs) are by far the oldest and  
 149 largest group of variable estimation approaches. VIs are defined to enhance spectral features  
 150 sensitive to a vegetation property, while reducing disturbances by combining some spectral  
 151 bands into a VI (Clevers, 2014; Glenn et al, 2008). The main advantage of VIs is their in-  
 152 trinsic simplicity. VI-based methods found their origin in the first applications of broadband  
 153 sensor satellites. During the pioneering years of optical remote sensing only a small set of  
 154 spectral bands were available and computational power was limited. It led to a long tradition  
 155 of the development of simple two-bands, or at most three to four band indices that continues  
 156 until today (e.g. Kira et al, 2016). New possibilities have opened with the advent of imaging  
 157 spectrometers. Optimized narrowband information extraction algorithms were developed  
 158 based on adaptations of established index formulations, such as simple ratio, normalized  
 159 difference (see reviews Clevers (2014); Glenn et al (2008); Xue and Su (2017)). On the  
 160 other hand, the possibilities to develop spectral indices based on a few band combinations  
 161 grew exponentially, and it demanded for more systematic band evaluation methods.

162 A popular solution involves correlating all possible band combinations according to estab-  
 163 lished index formulations. For two-band index formulations, such as simple ratio or normal-  
 164 ized difference, this approach leads to 2D correlation matrices, which enables to visually  
 165 identify optimal band combinations (e.g. Atzberger et al, 2010; le Maire et al, 2004, 2008;  
 166 Mariotto et al, 2013; Rivera et al, 2014; Thenkabail et al, 2000). Subsequently, given all  
 167 possible combinations permits to select a 'best performing index'. Nevertheless, while be-  
 168 ing mathematically simple, this method is not only tedious – especially when evaluating

169 all possible combinations of more than two bands – but also keeps on being restricted to  
170 formulations that make use of a few bands only, with at most using three or four bands.  
171 Thus, although the approach is systematic, it continues to underexploit the comprehensive  
172 information content hidden in the contiguous spectral data. Moreover, when applying this  
173 technique in mapping applications making use of imaging spectroscopy, identical best per-  
174 forming spectral band combinations for the same biophysical variable have rarely been re-  
175 ported. This suggests that optimized narrowband VIs are strongly case specific and seem to  
176 lack generic capacity (Gonsamo, 2011; Heiskanen et al, 2013; Mariotto et al, 2013).  
177 More fundamentally, it remains dubious whether relying on transformed data originating  
178 from a few discrete bands fully captures the complexity of real world observation conditions  
179 as has been observed by a spectroradiometer. Reducing full-spectrum datasets into simple  
180 indices formulations intrinsically leads to remaining spectral information left unexploited.  
181 Accordingly, the following two aspects should be considered to ensure optimized use of VIs  
182 in a spectroscopic context: (1) *Band selection*. Spectral indices are mathematical functions  
183 based on discrete bands, or at best a subset of full spectral information. Thus, the question  
184 arises: how do we assess with high enough accuracy whether the most sensitive spectral  
185 bands – with respect to biophysical variable retrieval – have been selected? (2) *Formulation*.  
186 Enhancing spectral information according to a mathematical transformation should lead to  
187 an optimal sensitivity of the spectral signal with respect to the variable of interest. While  
188 established formulations such as the simple ratio or normalized difference are commonly  
189 used, here the question arises again: how can we be sure whether these linear formula-  
190 tions are the most powerful ones with respect to biophysical variable retrieval? These two  
191 questions are almost impossible to resolve considering the unlimited possibilities of band  
192 selections together with designing index formulations. Consequently, given their inherent  
193 constraints, it can be concluded that VI-based regression models exploit spectroscopic  
194 data suboptimally.

## 195 2.2 Parametric approaches based on spectral shapes and spectral transformations

196 Because none of the above few-band indices methods take full advantage of spectroscopic  
197 datasets, alternative methods were pursued with the advent of hyperspectral spectroradiome-  
198 ters that allow to exploit specific absorption regions of the reflectance spectrum. It led to the  
199 development of so-called *shape* indices and spectral transformation methods. Shape indices,  
200 listed below, extract shape-related information from contiguous spectral signatures for a spe-  
201 cific spectral region that is then correlated with a biophysical variable. These types of para-  
202 metric methods are therefore exclusively applicable to spectroscopic data. The following  
203 categories can be identified:

204 – *Red-edge position (REP) calculations*. Mathematically, the REP inflection point is the  
205 position of a wavelength defined as the maximum of the first derivative reflectance be-  
206 tween the red and NIR regions, i.e., between 670 and 780 nm (Kanke et al, 2016). The  
207 red-edge position is known to be sensitive to multiple biophysical variable variations,  
208 both chlorophyll pigments (Delegido et al, 2011) as well as structural variables, for  
209 instance the leaf area index (LAI) (Delegido et al, 2013). Therefore, REP-related meth-  
210 ods are typically used to derive canopy chlorophyll content, being the product of LAI  
211 and leaf chlorophyll content (Clevers and Kooistra, 2012; Li et al, 2017). Many math-  
212 ematical approaches have been proposed to exploit this region as a sensitive indicator,  
213 including: (1) high-order curve fitting (Broge and Leblanc, 2001; Clevers et al, 2004);  
214 (2) inverted Gaussian models (Cho and Skidmore, 2006; Cho et al, 2008; Miller et al,  
215 1990); (3) linear interpolation and extrapolation methods (Cho et al, 2008; Tian et al,

- 216 2011); (4) Lagrangian interpolation (Dawson et al, 1998; Pu et al, 2003); (5) rational  
217 function application (Baranoski and Rokne, 2005); and more recently, (6) a wavelet-  
218 based technique (Li et al, 2017).
- 219 – *Derivative-based indices.* Although several of the above-described methods make use  
220 of derivatives, e.g. linear extrapolation (Cho and Skidmore, 2006) and Lagrangian tech-  
221 nique (Dawson et al, 1998), the calculation of a derivative does not have to be restricted  
222 to the red edge. The derivative of any spectral region can be calculated and transformed  
223 into an index (Elvidge and Chen, 1995; Penuelas et al, 1994; Sims and Gamon, 2002;  
224 Zarco-Tejada et al, 2002). A systematic comparison of first derivative-based indices and  
225 conventional indices was performed by le Maire et al (2004) using the leaf optical model  
226 PROSPECT. Interestingly, the authors concluded that derivative-based indices are not  
227 necessarily better than conventional and properly elaborated indices.
  - 228 – *Integration-based indices.* Alternatively, some authors proposed to calculate finite inte-  
229 grals of specific spectral regions, typically covering a part of the visible and the red-edge  
230 region for LAI or chlorophyll content estimations, into a (normalized) index (Broge  
231 and Leblanc, 2001; Delegido et al, 2010; Malenovský et al, 2006; Malenovský et al,  
232 2015; Mutanga et al, 2005; Opelet and Mauser, 2004). Likewise, in a recent study of  
233 Pasqualotto et al (2018) this method exploited the water absorption spectral regions to  
234 quantify canopy water content. In these studies, integration-based indices were demon-  
235 strated to perform superior to classical vegetation indices, as they exploit more optimally  
236 absorption regions embedded in spectroscopic data than indices relying on a reflectance  
237 intensity of few individual bands (Kováč et al, 2013). It can be expected that with the  
238 upcoming free availability of imaging spectroscopy data more of this kind of methods  
239 that explicitly exploit absorption features related to foliar constituents and pigments will  
240 emerge.
  - 241 – *Continuum removal.* Whereas the above techniques focus on one or more specific spec-  
242 tral regions, continuum removal is a spectral transformation that can be applied over  
243 the full spectrum. This technique normalizes reflectance spectra, allowing comparison  
244 of individual absorption features with a common baseline (Clark and Roush, 1984).  
245 The continuum removal transformation enhances and standardizes the specific absorp-  
246 tion features related to vegetation properties. Continuum removal can be considered as  
247 a standard spectroscopic data processing technique and has found its way in various  
248 image processing software packages. Spectroscopic examples of applications include  
249 mapping of chlorophyll (Broge and Leblanc, 2001; Malenovský et al, 2013; Malen-  
250 ovský et al, 2017), numerous studies on mapping nitrogen content (Huang et al, 2004;  
251 Mitchell et al, 2012; Mutanga and Kumar, 2007; Mutanga and Skidmore, 2004; Schlerf  
252 et al, 2010; Yao et al, 2015), foliar water condition (Stimson et al, 2005), plant stress  
253 (Sanches et al, 2014) and grassland biomass (Buchhorn et al, 2013; Cho et al, 2007).
  - 254 – *Wavelet transform.* Wavelet analysis has been increasingly used to extract information  
255 from spectral data, e.g. related to vegetation properties (Rivard et al, 2008). Processing  
256 of reflectance spectra with wavelets can be performed as discrete or continuous (CWT)  
257 transforms. CWT outputs are directly comparable to the original spectrum and are sim-  
258 ple to interpret. In this case, the original spectrum is represented by a set of spectra from  
259 small (narrow bandwidth absorption feature and noise) to larger scales (broad features,  
260 continuum). By selecting small scale spectra (i.e. discarding the smallest scale, which  
261 contains white noise and high scales related to the continuum), the absorption features  
262 of the components are enhanced, preserving the spectral information of the original data  
263 (Scafutto et al, 2016). Based on the type of wavelet transform, specific bands sensitive  
264 to the targeted variable are then selected (Bao et al, 2017). CWT is often compared in  
265 spectroscopic studies against spectral indices and was found to be capable of delivering

266 stronger correlations, e.g. in the detection of wheat aphid pests (Luo et al, 2013), LAI  
 267 estimation (Huang et al, 2014), nitrogen content and chlorophyll content estimation (He  
 268 et al, 2015; Kalacska et al, 2015; Luo et al, 2013) and in amplifying spectral separability  
 269 of alpine wetland grass species. (Bao et al, 2017).

270 Altogether, correlations based on shape indices and spectral transformations are undoubt-  
 271 edly more sophisticated normalization approaches than traditional spectral indices for ex-  
 272 ploiting the spectral information embedded in spectroscopic data. Moreover, their rela-  
 273 tively simple mathematical formulation ensures fast processing. It seems thus logical that  
 274 these spectral transformation methods became standard spectroscopy image processing tech-  
 275 niques. However, these methods alone provide nothing more than spectral transformations  
 276 and enhancements. When aiming to estimate a biophysical variable, a fitting function – typ-  
 277 ically a linear least squares fitting, but also exponential, power and polynomial – is still re-  
 278 quired. Yet it remains questionable whether the selected fitting function is the most suitable  
 279 one. Moreover, since parametric approaches are based on relatively simple mathematical  
 280 definitions – as opposed to more advanced methods – no associated uncertainty intervals  
 281 are provided. Although their strengths lie in their straightforward use and fast processing,  
 282 with the absence of a per-pixel uncertainty estimate, the performance quality of parametric  
 283 regression methods as a mapping method is hard to judge. Given the surface diversity cap-  
 284 tured in a single airborne or spaceborne image, and despite a standard validation exercise for  
 285 a number of pixels, it still remains unknown how the retrieval quality evolves throughout a  
 286 complete image. The absence of a quality indicator is, therefore, in our view the main reason  
 287 why parametric regression methods are not recommendable for operational quantification of  
 288 biophysical variables.

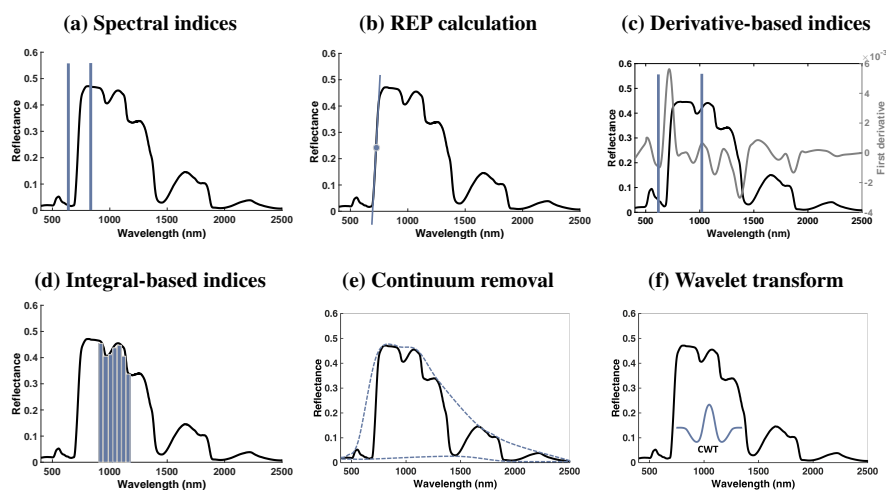


**Fig. 2** Schematic representation of parametric regression methods: Spectral indices (a), Red-edge position (REP) calculation (b), derivative-based indices (c), integral-based indices (d) continuum removal (e), and wavelet transform (f). Note that a fitting function is still required to convert these transformations towards a biophysical variable.

### 289 3 Non-parametric regression methods

290 Contrary to parametric methods, non-parametric methods optimize the regression algo-  
 291 rithm by means of an inherent learning phase based on training data. Essentially, the non-  
 292 parametric model develops weights (coefficients) adjusted to minimize the estimation error  
 293 of the variables extracted. This means that no explicit parametrization is required, which  
 294 practically simplifies the model development, but more expert knowledge to understand  
 295 and execute these models may be required. Another important advantage of non-parametric  
 296 methods is the possibility of training with the full-spectrum information. Hence, an explicit  
 297 selection of spectral bands or transformations is in principle not required. A flexible model  
 298 is able to combine different data structure features in a nonlinear manner to conform re-  
 299 quirements; however model definition with a too flexible capacity may incur the problem of  
 300 over-fitting the training dataset. To avoid this pitfall, model weights are defined by jointly  
 301 minimizing the training set approximation error while limiting the model complexity. In  
 302 view of processing spectroscopic data, a more prevalent problem lies in the so-called *curse*  
 303 *of dimensionality* (Hughes phenomenon) (Hughes, 1968). Adjacent, contiguous bands carry  
 304 highly intercorrelated information, which may result in redundant data and possible noise  
 305 and potentially suboptimal regression performances. As discussed further on, band selection  
 306 or dimensionality reduction methods that transform the spectral data to lower-dimensional  
 307 space, while containing the vast majority of the original information can overcome this  
 308 problem.

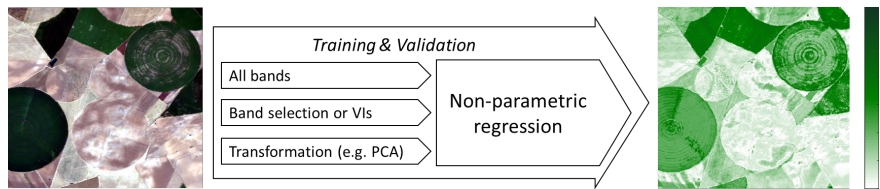


**Fig. 3** Principles of non-parametric regression. Left: RGB subset of a hyperspectral HyMap image (125 bands) over Barrax agricultural site (Spain). Right: illustrative map of a vegetation property (LAI,  $\text{m}^2/\text{m}^2$ ) as obtained by PROSAIL with Gaussian processes regression (GPR). The model was validated with a  $R^2$  of 0.94 (RMSE: 0.39; NRMSE: 6.3%). It took 5.7 seconds to produce the map using ARTMO's MLRA toolbox (Rivera Caicedo et al, 2014). With GPR also uncertainty estimates are provided (not shown).

#### 309 3.1 Linear non-parametric methods

310 Non-parametric regression algorithms that apply linear transformations are attractive be-  
 311 cause of their fast performance. These methods became standard methods in chemometric  
 312 and in image processing software packages. Multivariable linear regression methods can  
 313 cope with spectroscopic data and typically rely on the estimation of co-variances. When  
 314 moving towards spectroscopic data, however, this can become problematic when input data  
 315 quantity is limited with respect to the dimensionality of the dataset. To alleviate collinear-  
 316 ity, often linear non-parametric methods are applied in combination with a dimensionality  
 317 reduction step. Some methods are even intrinsically based on this principle, i.e. principal  
 318 component regression (PCR) (Wold et al, 1987), and partial least squares regression (PLSR)  
 319 (Geladi and Kowalski, 1986). Common linear non-parametric regression approaches are  
 320 provided in table 1 and imaging spectroscopy applications are discussed below.



**Table 1** Linear non-parametric regression methods applicable to spectroscopic data.

Method	Description	Ref.
Stepwise multiple linear regression (SMLR)	SMLR recursively applies multiple regression a number of times. Each step removes a variable eliciting the weakest correlation. At the end of the recursive process, a variable set is obtained that is optimally explaining the spectral data distribution.	Draper and Smith (2014)
Principal components regression (PCR)	PCR is a regression analysis method based on principal components analysis (PCA) estimating regression coefficients. Solutions from PCR are generated performing linear regression of the most relevant components (called scores) obtained after applying PCA.	Wold et al (1987)
Partial least squares regression (PLSR)	PLSR is similar as PCR but tackles the co-linearity problem differently than PCR. Applying PCR, regression is performed using PCA scores. These projections are obtained using only input patterns, not outputs. In contrast, PLSR builds the regression model on projections obtained using the partial least squares (PLS) approach. It elicits the directions of maximum input-output cross-covariance. Therefore, PLSR takes both input patterns and output variables into account.	Geladi and Kowalski (1986)
Ridge (regulated) regression (RR)	RR is the most commonly used method of regularization for ill-posed problems, which are problems that do not have a unique solution. RR deals with co-linearity by allowing a degree of bias in the estimates. Therefore, RR adds a small positive value $\lambda$ to the diagonal elements of the input data covariance matrix. Hence, RR requires finding an optimal value for $\lambda$ . Typically, cross-validation is used to reach near optimal values. An important fact about RR is that it enforces the regression coefficients to be lower, but it does not enforce them to be zero. That is, it will not get rid of irrelevant features (bands) but rather minimize their impact on the trained model.	Geladi and Kowalski (1986)
Least absolute shrinkage and selection operator (LASSO)	Lasso is an extension built on RR, but with a small twist. It also penalizes the regression coefficients absolute size. By this penalization some of the variable estimates may be exactly zero. The larger the penalty, the more the estimates will tend toward zero. This is a convenient approach to automatically perform feature selection, or to deal with correlated predictors.	Tibshirani (1996)

321 On the application side, stepwise multiple linear regression (SMLR) is a classical multivari-  
322 able regression algorithm commonly applied in chemometrics (Atzberger et al, 2010). To  
323 evaluate its predictive power, SMLR has been often compared with alternative regression  
324 techniques such as PLSR and some studies concluded that PLSR yielded better results when  
325 estimating LAI (Darvishzadeh et al, 2008) and canopy chlorophyll content (Atzberger et al,  
326 2010). Also Ramoelo et al (2011) compared both regression algorithms to estimate foliar ni-  
327 trogen and phosphorus in combination with continuum removal using field spectrometry. By  
328 estimating canopy nitrogen, Miphokasap et al (2012) demonstrated that the model developed  
329 by SMLR led to a higher correlation coefficient and lower errors than model applications  
330 based on narrowband VIs. This suggests that non-parametric (full-spectrum) models tend to  
331 be more powerful than parametric models. Likewise, Yi et al (2014) compared SMLR with  
332 PLSR and spectral indices for carotenoid estimation in cotton and concluded that best esti-  
333 mations were obtained with PLSR. Likewise, SMLR was compared with PLSR and (nonlin-  
334 ear) machine learning regression algorithms for estimating leaf nitrogen content (Yao et al,  
335 2015). Because of their enhanced flexibility, it may not be a surprise that the nonlinear meth-  
336 ods outperformed SMLR and PLSR. This was also observed by various similar studies, as  
337 will be addressed in section 3.2.

338 PCR seems to be more effective in the conversion of spectroscopic data into the estimation  
339 of vegetation properties, because the PCA-based dimensionality reduction method is embed-  
340 ded in the method in combination with a linear regression function. Hence, by converting  
341 the spectral data to a lower dimensional space automatically overcomes the band redundancy  
342 problem. This method has been improved with PLSR, where the projections are optimized in  
343 view of the regression. It is, therefore, not a surprise that only few spectroscopic studies ex-  
344 amined the predictive power of PCR. Those studies compared PCR against PLSR or against  
345 VIs (Atzberger et al, 2010; Fu et al, 2012; Marshall and Thenkabail, 2014; Rivera Caicedo  
346 et al, 2014; Wang et al, 2017b). Although PCR generally outperformed VIs in explaining

347 variability of a vegetation attribute, in all cases PLSR or any other non-parametric method  
348 overran PCR.

349 PLSR found its way in a broad diversity of imaging spectroscopy applications, especially  
350 in the mapping of biochemicals, pigments and vegetation density properties. For instance,  
351 PLSR was used in several spectroscopic studies applied to estimate foliage nitrogen content  
352 (Coops et al, 2003; Hansen and Schjoerring, 2003; Huang et al, 2004). Also Gianelle and  
353 Guastella (2007) used PLSR to derive grassland phytomass and its total (percentage) nitro-  
354 gen content from spectroscopic data. Similarly, Cho et al (2007) and Im et al (2009) applied  
355 PLSR to estimate a diversity of grass and crop biophysical variables (LAI, stem biomass and  
356 leaf nutrient concentrations), and Ye et al (2007) applied PLSR for yield prediction purposes.  
357 Beyond individual vegetation attributes, PLSR was recently used to predict landscape-scale  
358 fluxes of net ecosystem exchange (NEE) and gross primary productivity (GPP) across mul-  
359 tiple timescales (Matthes et al, 2015), and also for the estimation of floristic composition  
360 of grassland ecosystems (Harris et al, 2015; Neumann et al, 2016; Roth et al, 2015). At the  
361 same time, thanks to its PLS-vectors, PLSR is also increasingly applied for band sensitivity  
362 analysis of spectroscopic datasets in view of the targeted application (e.g. Feilhauer et al,  
363 2015; Kiala et al, 2016; Kira et al, 2016; Li et al, 2014a; Neumann et al, 2016). Various  
364 experimental studies demonstrated the superior predictive power of PLSR as opposed to  
365 VIs for the prediction of multiple vegetation properties, including above-ground biomass,  
366 LAI, leaf pigments (chlorophyll, carotenoids), GPP and NEE fluxes, leaf rust disease detec-  
367 tion and nutrients concentration (nitrogen and phosphorus concentrations) (Capolupo et al,  
368 2015; Dreccer et al, 2014; Foster et al, 2017; Hansen and Schjoerring, 2003; Matthes et al,  
369 2015; Wang et al, 2017a; Yue et al, 2017). However, when compared against machine learn-  
370 ing methods, then PLSR no longer appeared to be top performing (Ashourloo et al, 2016;  
371 Kiala et al, 2016; Wang et al, 2015; Yao et al, 2015). As will be addressed in section 3.2,  
372 this is due to the nonlinear transformation conducted in machine learning methods.

373 Other linear non-parametric regression methods, such as ridge regression (RR) and LASSO,  
374 hardly made it into applications for vegetation properties mapping. Yet a few spectroscopic  
375 examples are worth mentioning. For instance, Addink et al (2007) used RR to map LAI  
376 and biomass, and more recently Bratsch et al (2017) applied LASSO to estimate above-  
377 ground biomass quantities among different plant tissue type categories in Alaska. In another  
378 biomass estimation study, both RR and LASSO were compared against PLSR (Lazaridis  
379 et al, 2010) and also random forests (Zandler et al, 2015). Interestingly, RR and LASSO  
380 appeared to be top performing. One may, therefore, wonder why these techniques have not  
381 been applied more often. On the other hand, these linear methods are increasingly replaced  
382 by their nonlinear counterparts. For instance, RR has been replaced by kernel ridge regres-  
383 sion (KRR) (Suykens and Vandewalle, 1999), and also PLSR has been redesigned into a  
384 kernel version, i.e. the KPLSR, which proved to be more powerful than PLSR for chloro-  
385 phyll concentration estimation (Arenas-García and Camps-Valls, 2008). The family of ker-  
386 nel methods is addressed in section 3.2. That none of these linear methods deliver uncer-  
387 tainty estimates is another drawback. Similar as in case of parametric regression, without  
388 uncertainty estimates it remains questionable whether these methods can deliver consistent  
389 mapping quality throughout a complete image, or are applicable to other images in space  
390 and time.

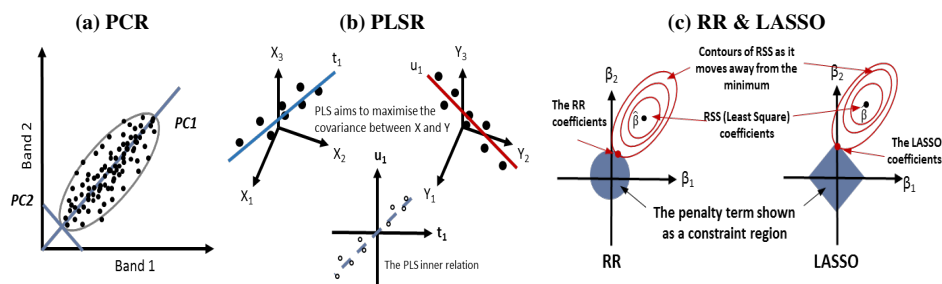


**Fig. 4** Schematic representation of principal component (PC) (a), partial least squares (PLS) (B), ridge regression and LASSO (c). PC and PLS is combined with a linear regression model.

### 391 3.2 Nonlinear non-parametric models

392 When advancing beyond linear transformation techniques, a diversity of nonlinear non-  
 393 parametric models has been developed during last few decades. These methods, also referred  
 394 to as machine learning regression algorithms, apply nonlinear transformations. An  
 395 important methodological advantage is their capability to capture nonlinear relationships of  
 396 image features without explicitly knowing the underlying data distribution. Hence, they are  
 397 developed without assuming a particular probability density distribution, which is the reason  
 398 why they work well with all kinds of data types. Machine learning methods also offer  
 399 the possibility to incorporate a prior knowledge and the flexibility to include different data  
 400 types into the analysis. In principle they are perfectly suited to process spectroscopic data.  
 401 In the following sections, examples of the families of (1) decision trees, (2) artificial neural  
 402 networks and (3) kernel-based regression are explained.

#### 403 3.2.1 Decision trees

**Table 2** Decision tree regression methods applicable to spectroscopic data.

Method	Description	Ref.
Decision trees (DT)	DT learning is based on decision tree predictive modeling. A decision tree is based on a set of hierarchical connected nodes. Each node represents a linear decision based on a specific input feature.	Breiman et al (1984)
Boosted trees (BoT)	BoT Incrementally builds an ensemble by training each new instance to emphasize the training instances previously mis-modeled.	Friedman et al (2000)
Bagging trees (BaT)	BaT an early ensemble method based on building multiple decision trees by iteratively replacing resampled training data and voting for the decision trees leading to a consensus prediction.	Breiman (1996)
Random Forests (RF)	RF is a specific type of BaT that in constructs a collection of decision trees with controlled variance.	Breiman (2001)

404 Decision tree algorithms use a branching method to illustrate every possible outcome of a  
 405 decision (for examples see Table 2). They are more frequently applied in classification than  
 406 in regression. Only a few decision tree feasibility studies dealing with imaging spectroscopy  
 407 data are presented in the scientific literature (e.g. Im et al, 2009) most likely because boosted  
 408 and bagging trees hardly found their way to regression applications. They might be considered  
 409 as obsolete with the improvements introduced into random forests (RF), which is  
 410 essentially a specific type of bagging trees. **RF builds an ensemble of individual decision**

411 trees working with different subsets of features (bands) and eventually different training  
 412 data points both selected randomly, from which a final prediction is made using particular  
 413 combination schemes. RF can handle a large number of training samples, does not suffer  
 414 from overfitting and is robust to outliers and noise (Belgiu and Drăguț, 2016), which makes  
 415 it an attractive method for spectroscopic mapping applications. RF has recently been made  
 416 available in various software packages and proved to be a competent regression algorithm.  
 417 It therefore comes as no surprise that RF gained rapid popularity in imaging spectroscopy  
 418 mapping of a diverse range of vegetation attributes, including biomass (Adam et al, 2014;  
 419 Vaglio Laurin et al, 2014), canopy nitrogen (Li et al, 2014b) and as indicator of plant species  
 420 composition (Feilhauer et al, 2017). Some of these studies have compared RF with support  
 421 vector regression (SVR) or neural networks, but no strong preference towards one or the  
 422 other method was found, which suggests that all three methods are competitive (Han et al,  
 423 2016; Pullanagari et al, 2016). However, just like other machine learning regression meth-  
 424 ods, RF can face difficulties coping with the collinearity of the spectroscopic data (Rivera-  
 425 Caicedo et al, 2017). To overcome this problem, RF is often used in combination with sensi-  
 426 tive bands or simple transformations in the form of VIs that are known to be sensitive to  
 427 the targeted vegetation property (Adam et al, 2014; Han et al, 2016; Liang et al, 2016). Al-  
 428 ternatively, RF is inherently able to identify sensitive spectral bands, and selection of only  
 429 those sensitive bands can subsequently improve the regression model (Balzarolo et al, 2015;  
 430 Feilhauer et al, 2015). Whether applying a band selection method is the most successful  
 431 strategy, however, remains an open question. Rather than seeking for optimized individual  
 432 bands, a more elegant solution may lie in firstly applying dimensionality reduction method,  
 433 and then inputting the features of the lower-dimensional space (i.e., components) into the  
 434 decision tree (Rivera-Caicedo et al, 2017).

### 435 3.2.2 Artificial neural networks

**Table 3** Artificial neural network regression methods applicable to spectroscopic data.

Method	Description	Ref.
Artificial neural networks (ANN)	ANNs in their basic form are essentially fully connected layered structures of artificial neurons (AN). An AN is basically a pointwise nonlinear function (e.g., a sigmoid or Gaussian function) applied to the output of a linear regression. ANs with different neural layers are interconnected with weighted links. The most common ANN structure is a feed-forward ANN, where information flows in a unidirectional forward mode. From the input nodes, data pass hidden nodes (if any) toward the output nodes.	Haykin (1999)
Back-propagation ANN (BPANN)	The he basic type of neural network is multi-layer perceptron, which is feed-forward back-propagation ANN. BPANN consists of 2 steps: 1) feed forward the values, and 2) calculate the error and propagate it back to the earlier layers. So to be precise, forward-propagation is part of the backpropagation algorithm but comes before back-propagating. This is the most common used algorithm when referring to ANN. In many papers using ANN these standard designs are not explicitly mentioned.	Haykin (1999)
Radial basis function ANN (RBFANN)	RBFANN is a type of ANN that uses non-linear radial basis functions (RBF) as activation functions in the hidden layer. The output of the network is a linear combination of RBFs of the inputs and neuron parameters.	Broomhead and Lowe (1988)
Recurrent ANN (RANN)	A RANN is a type of ANN that make use of sequential information by introducing loops in the network.	Hochreiter and Schmidhuber (1997)
Bayesian regularized ANN (BRANN)	BRANNs are more robust than standard BPANNs and can reduce or eliminate the need for lengthy cross-validation. Bayesian regularization is a mathematical process that converts a nonlinear regression into a "well-posed" statistical problem in the manner of a ridge regression.	Burden and Winkler (1999)

Artificial neural networks (ANNs) methods are listed in table 3. Since the early 90s, feed-forward and back-propagation ANNs thrived in all kinds of mapping applications, including vegetation properties mapping (Francel and Panigrahi, 1997; Kimes et al, 1998; Paruelo and Tomasel, 1997). Their strengths lie in their adaptability that can lead to excellent performances. The superiority of ANNs in vegetation properties mapping compared to parametric models (e.g. those based on VIs) has been demonstrated repeatedly in experimental studies (Kalacska et al, 2015; Malenovský et al, 2013; Uno et al, 2005; Wang et al, 2013). Examples of successful spectroscopic applications include the estimation of foliage nitrogen concentrations (Huang et al, 2004) and LAI (Jensen et al, 2012; Neinavaz et al, 2016). In both cited studies, ANN outperformed other linear non-parametric models (e.g. PLSR). Alternative powerful structures involve RBFANNs, BRANNs and RANNs (for explanation see table 3). Although these advanced ANNs have been primarily used for classification applications, only recently they were explored to map vegetation properties from spectroscopic data (Chen et al, 2015; Feng et al, 2016; Pôças et al, 2017; Wang et al, 2013). Some of these studies mention the superiority of these advanced ANN designs as compared to standard ANN designs or other machine learning approaches in estimating vegetation properties (Du et al, 2016; Li et al, 2017; Pham et al, 2017).

Applying ANNs to spectroscopic data, nonetheless, can be quite challenging due to the multicollinearity. Feeding many bands into an ANN requires a complex design and consequently a long training time. Just as with decision trees, a popular approach is applying a band selection or the calculation of several sensitive VIs or shape indices such as red edge position that are then entered either individually or as a combination into the ANN. Various of these band selection studies investigated combinations of VIs that led to best prediction models (Chen et al, 2015; Feng et al, 2016; Jia et al, 2013; Liang et al, 2015; Mutanga and Kumar, 2007; Pôças et al, 2017; Schlerf and Atzberger, 2006). As discussed before, it remains questionable whether the selected indices preserve a maximum amount of useful information. In contrary, when compressing the spectral data using dimensionality reduction methods into a lower-dimensional space, then it is ensured that a maximum amount of spectral information is preserved. This approach was applied e.g. to assess corn yield (Uno et al, 2005) and phosphorus and nitrogen concentrations (Knox et al, 2011). It is therefore not surprising that a study comparing PCA vs. indices inputted into ANNs concluded that the PCA-ANN design outperformed VI-ANN designs (Liu and Pan, 2017). Moreover, given that only linear transformations are applied in PCA, it may even be that more adaptive dimensionality reduction methods yield superior accuracies when combined with ANN, e.g. partial least squares (PLS), or in the field of nonlinear kernel-based dimensionality reduction methods, e.g. kernel PCA (KPCA) or kernel PLS (KPLS). To ascertain this hypothesis, PCA was compared against 10 alternative dimensionality reduction methods in combination with ANN to carry out LAI estimation. As expected, various alternative dimensionality reduction methods outperformed PCA in developing accurate models (e.g., PLS, KPLS, KPCA) (Rivera-Cacedo et al, 2017).

### 3.2.3 Kernel-based machine learning regression methods

Kernel-based regression methods solve nonlinear regression problems by transferring the data to a higher-dimensional space by a kernel function (Table 4). The flexibility offered by kernel methods allows to transform almost any linear algorithm that can be expressed in terms of dot products, while still using only linear algebra operations. Kernel methods provide a consistent theoretical framework for developing nonlinear techniques and have useful properties when dealing with a low number of (potentially high dimensional) training samples, and outliers and noise in the data (Gómez-Chova et al, 2011; Tuia et al, 2018). Given

**Table 4** Kernel-based regression methods applicable to spectroscopic data.

Method	Description	Ref.
Support vector regression (SVR)	The Support Vector Machine (SVM) is a supervised machine learning technique that was invented in the context of the statistical learning theory. It was not until the mid-90s that an algorithm implementation of the SVM was proposed with the introduction of the kernel trick and the generalization to the non-separable case. SVR is built on the principle of SVM: a non-linear function is learned by linear learning machine mapping into high dimensional kernel induced feature space. The capacity of the system is controlled by parameters that do not depend on the dimensionality of feature (bands) space.	Vapnik et al (1997)
Kernel ridge regression (KRR)	KRR combines RR with the kernel trick. It thus learns a linear function in the space induced by the respective kernel and the data. For non-linear kernels, this corresponds to a non-linear function in the original space. The form of the model learned by KR is identical to SVR. However, different loss functions are used: KRR uses squared error loss while SVR uses $\epsilon$ -insensitive loss combined with RR regularization.	Suykens and Vandewalle (1999)
Gaussian process regression (GPR)	GPR is based on Gaussian processes (GPs), which generalize Gaussian probability distributions in a function's space. A GP is stochastic since it describes the properties of functions. As in Gaussian distributions, a GP is described by its mean (which for GPs is a function) and covariance (a kernel function). This represents an expected covariance between function values at a given point. Because a GPR model is probabilistic, it is possible to compute the prediction intervals using the trained model.	Rasmussen and Williams (2006)

484 these attractive properties, kernel-based regression methods seem perfectly suited to extract nonlinear information related to vegetation properties from imaging spectroscopy data.

485  
486 Developed in the mid-90s, among the most popular kernel-based method for classification purposes involves SVMs. Its regression version (SVR) gained popularity for the retrieval of  
487 continuous vegetation attributes from imaging spectroscopy data in the last decade. Examples  
488 include plant height, leaf nitrogen content, and leaf chlorophyll content (Karimi et al,  
489 2008; Yang et al, 2011). A multi-output version of SVR was presented by Tuia et al (2011),  
490 with LAI, leaf chlorophyll content and fractional vegetation content being simultaneously  
491 estimated. Recently, SVR was used for processing spectroscopic images of sub-decimeter  
492 spatial resolution as acquired by low-altitude unmanned aircraft system to infer Antarctic  
493 moss vigour (Malenovský et al, 2017). Yet just as with the other advanced regression  
494 methods, SVR face the same difficulties of coping with multicollinearity. Therefore, SVR  
495 has been commonly applied in combination with specific spectral subsets or VIs (Lin et al,  
496 2013; Marabel and Alvarez-Taboada, 2013), or with wavelet transforms (He et al, 2015).  
497 To deal with spectroscopic band redundancy, an advantage of SVR is that it allows band  
498 selection (analogous as PLSR and RF), which in principle allows the development of more  
499 optimized models (Feilhauer et al, 2015). On the other hand, it is likely that the combination  
500 with dimensionality reduction methods will lead to more powerful models (Rivera-Caicedo  
501 et al, 2017). To assess its predictive power, various spectroscopic studies compared SVR  
502 against similar methods such as SMLR or PLSR, although some band selection method appeared  
503 to be essential (Kiala et al, 2016; Wang et al, 2015; Yao et al, 2015). Conversely,  
504 when comparing SVR against other machine learning methods such as RF or GPR, then  
505 SVR no longer excelled (Pullanagari et al, 2016).  
506

507 Kernel ridge regression (KRR) emerged as one of the promising upcoming kernel-based  
508 regression methods, although only a few spectroscopic studies have used it. For instance,  
509 Wang et al (2011) compared KRR with linear non-parametric methods (multiple linear regression  
510 and PLSR) for LAI estimation. The authors concluded that KRR yielded the most accurate  
511 estimates. Also Peng et al (2011) used KRR for the detection of chlorophyll content. Apart  
512 from these two studies, the spectroscopy vegetation community may not yet be familiar with  
513 this method. Solely Rivera Caicedo et al (2014) had compared KRR against other machine  
514 learning algorithms applied to CHRIS (62 bands) and HyMap (125 bands) spectroscopic data  
515 for LAI mapping. In that study, KRR not only proved to be a very competitive regression  
516 algorithm, but also proved to be extremely fast. This is due to its relatively

517 simple design that requires only one hyperparameter to be tuned. Because of its simplicity,  
 518 another advantage is that KRR is capable to deal with collinearity; the method can cope  
 519 with thousands of contiguous bands. In fact, in the dimensionality reduction comparison  
 520 study tested with simulated (2100 bands) and HyMap data (Rivera-Caicedo et al, 2017),  
 521 KRR was the only regression method where dimensionality reduction methods did not lead  
 522 to improvements as compared to using all bands. In conclusion, KRR emerged as an attrac-  
 523 tive regression method due to its competitive performance, fast processing and easiness to  
 524 deal with spectroscopic data.

525 From all machine learning regression algorithms, probably the most exciting one is Gaus-  
 526 sian process regression (GPR). Contrary to other methods, the training phase in GPR takes  
 527 place in a Bayesian framework, leading to probabilistic outputs (Camps-Valls et al, 2016;  
 528 Rasmussen and Williams, 2006). GPR applied to spectroscopic data started only recently,  
 529 e.g. for airborne HyMap mapping of leaf chlorophyll content (Verrelst et al, 2013a), and  
 530 for spaceborne CHRIS mapping of leaf chlorophyll content, LAI and fractional vegetation  
 531 content (Verrelst et al, 2012a). Of interest is that along with these maps also maps of associ-  
 532 ated uncertainties (prediction intervals) were provided. Also with an Airborne Hyperspectral  
 533 Scanner (Roelofsen et al, 2014) applied GPR to map salinity, moisture and nutrient concen-  
 534 trations that in turn were used as inputs for plant association mapping. In the Rivera Caicedo  
 535 et al (2014) comparison paper, GPR outperformed the majority of other tested machine  
 536 learning methods for the prediction of leaf chlorophyll content and LAI from various spec-  
 537 troscopic datasets. Similarly, Ashourloo et al (2016) concluded that GPR yielded most ac-  
 538 curate leaf rust disease detection as compared to VIs, PLSR and SVR. However, GPR is  
 539 no exception in suffering from radiometric collinearity when many bands are included; and  
 540 related spectroscopic studies demonstrated that results can be further improved by combin-  
 541 ing GPR with band selection (Verrelst et al, 2016b) or with dimensionality reduction  
 542 methods (Rivera-Caicedo et al, 2017). At the same time, alternative GPR versions continue  
 543 to be developed within the machine learning community. For instance, Lazaro-Gredilla et al  
 544 (2014) refined the GPR method by proposing a non-standard variable approximation allow-  
 545 ing for accurate inferences in signal-dependent noise scenarios. The so-called variational  
 546 heteroscedastic GPR (VHGPR) appears to be an excellent alternative for standard GPR,  
 547 which was demonstrated on a CHRIS dataset where VHGPR outperformed GPR in leaf  
 548 chlorophyll content estimation.

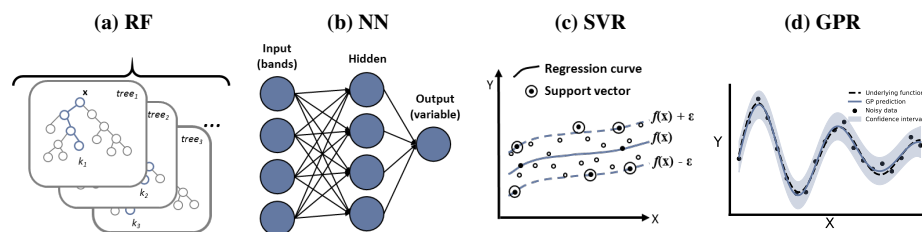


**Fig. 5** Schematic representation of Random forest (RF) (a), Neural networks (NN) (b), Support vector regression (SVR) (c), and Gaussian processes regression (GPR) (d).

#### 549 4 Physically-based model inversion methods

550 Physically-based model inversion is based on physical laws establishing cause-effect rela-  
 551 tionships. Inferences on model variables are based on generally accepted knowledge em-  
 552 bedded in radiative transfer models (RTMs). RTMs are deterministic models that describe

553 absorption and multiple scattering, and some of them even describe the microwave region,  
554 thermal emission or sun-induced chlorophyll fluorescence emitted by vegetation (e.g., see  
555 Table 5). A diversity of canopy RTMs have been developed over the last three decades with  
556 varying degrees of complexity. Gradual increase in RTMs accuracy, yet in complexity too,  
557 have diversified RTMs from simple turbid medium RTMs to advanced Monte Carlo RTMs  
558 that allow for explicit 3D representations of complex canopy architectures (e.g., see the  
559 RAMI exercises (Pinty et al, 2001, 2004; Widlowski et al, 2007, 2011, 2015) for a thorough  
560 comparison). This evolution has resulted in an increase in the computational requirements  
561 to run the model, which bears implications towards practical applications. From a compu-  
562 tational point of view, RTMs can be categorized as either (1) *economically invertible* (or  
563 computationally cheap); or as (2) *non-economically invertible* models (or computationally  
564 expensive). These terms refer to the model complexity and associated run-time constrain-  
565 ing the mathematical inversion of such models. Economically invertible models are models  
566 with relatively few input parameters and fast processing that enables fast calculations and  
567 consequently fast model inversion or rendering of simulated scenes. A well-known example  
568 of this category includes the widely used leaf RTM PROSPECT (Feret et al, 2008) coupled  
569 with the canopy RTM SAIL (Verhoef, 1984a) (combined named as PROSAIL (Jacquemoud  
570 et al, 2009a)).

571 Non-economically invertible RTMs refer to advanced, computationally-expensive RTMs,  
572 often with a large number of input variables and sophisticated computational and mathemat-  
573 ical modelling. These type of RTMs enable the generation of complex or detailed scenes, but  
574 at the expense of a significant computational load. In short, the following families of RTMs  
575 can be considered as non-economically invertible: (1) Monte Carlo ray tracing models (e.g.,  
576 Raytran (Govaerts and Verstraete, 1998), FLIGHT (North, 1996) and librat (Lewis, 1999));  
577 (2) voxel-based models (e.g., DART (Gastellu-Etchegorry et al, 1996)) and (3) advanced in-  
578 tegrated vegetation and atmospheric transfer models (e.g., SCOPE (Van Der Tol et al, 2009)  
579 and MODTRAN (Berk et al, 2006)). Descriptions of advanced canopy RTM models and  
580 their latest developments are provided in Table 5. Although these advanced RTMs serve  
581 perfectly as virtual laboratories for fundamental research on light-vegetation interactions,  
582 they are in general less suitable for retrieval applications, because of either a large number  
583 of input variables or a long processing time. Nevertheless, as outlined below, some exper-  
584 imental studies demonstrated that they can as well be applied into inversion schemes, e.g.  
585 based on look-up tables and in hybrid strategies.

586 Regardless of their complexity, they all deliver spectroscopic outputs, typically at 1 nm  
587 resolution. Hence, RTMs outputs can fit perfectly into inversion schemes of imaging spec-  
588 troscopy data, while at the same time the simulated data can be resampled to reassemble  
589 the band settings of multispectral sensors. Because inversion strategies are usually based on  
590 spectral fitting (i.e. only radiometric information is used), the drawback of collinearity com-  
591 plicating regression is not an issue here; however, removal of noisy bands is still a standard  
592 and much-needed preprocessing step to enable adequate spectral fitting. Another point to be  
593 mentioned is that inversion scheme can only retrieve the RTM input variables. Hence, using  
594 this strategy implies that only RTM state variables can be mapped. Yet because the RTM  
595 input variables drive the canopy absorbance and scattering mechanisms, the resulting output  
596 maps are considered to be physically sound (Knyazikhin et al, 2013; Myneni et al, 1995).

597 Given that in principle only a coupled leaf-canopy RTM and an inversion routine are re-  
598 quired for the retrieval of RTM state variables, the approach is generic and generally ap-  
599 plicable. Nevertheless, these approaches are not straightforward. First, an RTM has to be  
600 selected, whereby a trade-off between the realism and inversion possibility of the RTM has  
601 to be made. As discussed above, typically, complex models are more realistic, but they have  
602 many variables and consequently challenging to invert, whereas simpler models may be



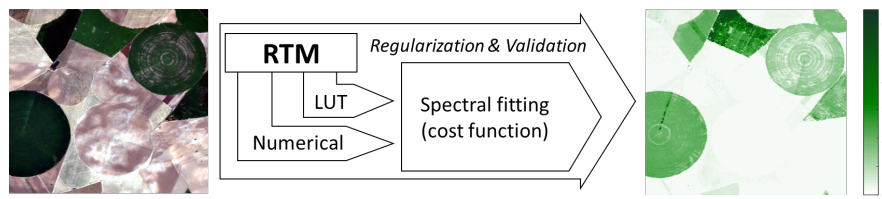


**Fig. 6** Principles of RTM inversion. Left: RGB subset of a hyperspectral HyMap image (125 bands) over Barrax agricultural site (Spain). Right: illustrative map of a vegetation property (LAI,  $\text{m}^2/\text{m}^2$ ) as obtained by RMSE inversion against a 100000 PROSAIL LUT (5% noise added, mean of 5% multiple solutions). The model was validated with a  $R^2$  of 0.44 (RMSE: 1.85; NRMSE: 31.9%). A systematic underestimation occurred, which in principle implies that the RTM simulated LUT needs to be better parameterized. It took 2315 seconds to produce the map using ARTMO's LUT-based inversion toolbox (Rivera et al, 2013). Also uncertainty estimates are provided, e.g. in the form of residuals (not shown).

603 less realistic but easier to invert. Secondly, according to the Hadamard postulates, RTMs  
 604 are invertible only when an inversion solution is unique and dependent – in a continuous  
 605 mode – on the variables to be extracted. Unfortunately, this boundary condition is often  
 606 not met. The inversion of canopy RTMs is frequently under-determined and ill-posed. The  
 607 number of unknowns can be much larger than the number of independent observations.  
 608 This makes physically-based retrievals of vegetation properties a challenging task. Several  
 609 strategies have been proposed to cope with the under-determined problem of optimizing the  
 610 inversion process, including (1) *iterative numerical optimization* methods, (2) *lookup-table*  
 611 (*LUT*) based inversion, or (3) *hybrid* approaches in which LUTs are generated as input for  
 612 machine learning approaches (see section 5). Below we briefly review some common RTM  
 613 inversion techniques in view of converting spectroscopic data into maps of RTM leaf and  
 614 canopy input variables.

615 *Numerical optimization*: Iterative optimization is a classical technique to invert RTMs in  
 616 image processing (Botha et al, 2007; Jacquemoud et al, 1995; Zarco-Tejada et al, 2001).  
 617 The optimization is minimizing a cost function, which estimates the difference between  
 618 measured and estimated variables by successive input variable iteration. Optimization al-  
 619 gorithms are computationally demanding and hence potentially time-consuming depending  
 620 on the complexity of the RTM and the numbers of image pixels to be processed. However,  
 621 with the ongoing increase in computational power and open-source availability of optimiza-  
 622 tion libraries, a renaissance of numerical approaches is emerging. Examples of numerical  
 623 inversion against spectroscopic data include: PROSPECT inversion to retrieve leaf chloro-  
 624 phyll content (Zhang and Wang, 2015), retrieval of leaf biochemistry against an improved  
 625 version of PROSPECT (COSINE) (Jay et al, 2016), and PROSAIL leaf and canopy vari-  
 626 ables (Bayat et al, 2016; van der Tol et al, 2016). Despite a gain in computational power,  
 627 numerical inversion algorithms applied to images are still time-consuming given the many  
 628 per-pixel iterations and a high number of pixels involved. Hence, in its current form this  
 629 method stays restricted to computationally fast RTMs in merely experimental settings.

630 *Look-up table (LUT)* strategies are based on the generation of simulated spectral reflectance  
 631 scenarios for a high number of plausible combinations of variable value ranges. As such,  
 632 the inversion problem is reduced to the identification of the modeled reflectance set that  
 633 resembles most closely the measured one. This process is based on querying the LUT and  
 634 applying a cost function. A cost function minimizes the summed differences between sim-  
 635 ulated and measured reflectances for all wavelengths. The main advantage of LUT-based  
 636 inversion routines over numerical optimization is their computational speed, since the com-  
 637 putationally most demanding part of the inversion procedure is completed before the inver-  
 638 sion itself (Dorigo et al, 2007). Consequently, LUT-based inversion methods are typically

**Table 5** Advanced canopy RTMs commonly used in imaging spectroscopy applications.

RTM	Description
SCOPE(Soil-Canopy-Observation of Photosynthesis and Energy fluxes)	SCOPE (Van Der Tol et al, 2009) is a Soil-Vegetation-Atmosphere (SVAT) scheme that includes RTMs along with a micrometeorological model for simulating turbulent heat exchange, and a plant physiological model for photosynthesis (Van Der Tol et al, 2014). The radiative transfer scheme is based on SAIL (Verhoef, 1984b, 1985), extended with a similar radiative transfer for emitted radiation. The emitted radiation includes chlorophyll fluorescence and thermal radiation. Leaf radiative transfer is calculated with Fluspect (Vilfan et al, 2016) which also includes emitted fluorescence radiation. SCOPE is intended as tool to scale processes from leaf to canopy, and to analyse the effects of light scattering. Recent developments include vertical heterogeneity (Yang et al, 2017) and the zeaxanthin-violaxanthin pigment cycles.
Discrete Anisotropic Radiative Transfer (DART)	DART model is being developed since 1992 as a physically based 3D computer programme (Gastellu-Etcheberry et al, 1996), which simulates radiative budget and remote sensing (airborne and spaceborne) optical image data of natural and urban landscapes for any wavelengths from the ultraviolet to the thermal infrared part of the electromagnetic spectrum (Gastellu-Etcheberry et al, 1999; Guillevic et al, 2003). It computes and provides bottom and top of the atmosphere spectral quantities (i.e., irradiance, exitance and radiance) that are transformed into reflectance or brightness temperature depending on the user DART mode preferences (Gastellu-Etcheberry et al, 2004). Simulated scenes may include the atmosphere, topography and any natural or anthropogenic objects at any geographical location (Grau and Gastellu-Etcheberry, 2013). The latest DART optical development includes also the specular reflectance and the light polarization (Gastellu-Etcheberry et al, 2015). Apart of passive remote sensing data, it also simulates active terrestrial and air-/space-borne light detection and ranging (LiDAR) discrete return, full waveform, multi-pulse and photon counting measurements (Gastellu-Etcheberry et al, 2016; Yin et al, 2016). In case of vegetation, it can also simulate radiative transfer of the solar-induced chlorophyll fluorescence for any virtual 3D Earth scene numerically and as images (Gastellu-Etcheberry et al, 2017).
librat	librat is a 3D Monte Carlo ray tracing radiative transfer model developed as a library interface to the original ararat (Advanced RAdiometric RAY Tracer) model. The first version of ararat was published in 1992 (Lewis and Muller, 1993) as part of the Botanical Plant Modelling System (BPMS) (Lewis, 1999; Lewis and Muller, 1990). Subsequently, the sampling scheme was improved as reported in Saich et al (2002), and the codes developed into a library in recent years. librat reads a 3D description of (canopy/soil/topographic) geometry, along with associated information on material scattering properties. The main function in the library then is that a ray is launched from some origin in 3D space, in a specified direction, and the code returns all information about the associated scattering paths and interactions, separated as direct and diffuse components. This core functionality, along with a set of associated sensor models but integrating paths fired into some volume. It allows for a wide range of radiative transfer calculations, including time-resolved/lidar, splitting of the radiometric information per scattering order etc. as well as straightforward reflectance/transmittance calculations (e.g. Disney et al, 2006; Hancock et al, 2012).
FLIGHT	FLIGHT (Barton and North, 2001; North, 1996) is a Monte Carlo ray tracing model designed to rapidly simulate light interaction with 3D vegetation canopies at high spectral resolution, and produce reflectance spectra for both forward simulation and for use in inversion (Leonenko et al, 2013). Foliage is represented by structural properties of leaf area, leaf angle distribution, crown dimensions and fractional cover, and the optical properties of leaves, branch, shoot and ground components. The model represents multiple scattering and absorption of light within the canopy and with the ground surface. It has been developed to model 3D canopy photosynthesis (Alton et al, 2007), to simulate waveform and photon counting lidar (Montesano et al, 2015; North et al, 2010) and emitted fluorescence radiation (Hernández-Clemente et al, 2017). Structural data may be specified as a statistical distribution, derived from field measurements (Morton et al, 2014) or by direct inversion from LiDAR data (Bye et al, 2017).

639 used as a preferred solution in RTM inversion studies. The classical LUT-based inversion  
640 approach is based on a RMSE cost function, which continues to be applied until today. This  
641 approach proved to be especially successful for chlorophyll (Kempeneers et al, 2008; Omari  
642 et al, 2013; Zhang et al, 2008) and LAI mapping. For instance, by using LUT-based inver-  
643 sion routines imaging spectroscopy data has been processed for the mapping of forest LAI  
644 (Banskota et al, 2013, 2015), grassland LAI (Atzberger et al, 2015) and LAI over agricul-  
645 tural crops based on UAVs (Duan et al, 2014). To further mitigate the ill-posed problem and  
646 optimize the robustness of the LUT-based inversion routines, a diversity of regularization  
647 strategies have been explored in inversion applications against spectroscopic data:

- 648 – *The use of prior knowledge* to constrain model variables in the development of a LUT  
649 (Baret and Buis, 2008; Darvishzadeh et al, 2008; Koetz et al, 2005). Prior knowledge  
650 typically involves information on the feasible variable ranges for involved vegetation

- 651 types (Dorigo et al, 2009; Verrelst et al, 2012c). Prior information together with prior  
652 distributions are also increasingly applied into a Bayesian context, whereby the inverted  
653 values are generated based on likelihoods (Laurent et al, 2013, 2014; Shiklomanov et al,  
654 2016). The advantage of a Bayesian framework is its capability to quantify an inversion  
655 uncertainty around an inversion variable.
- 656 – *Selection of cost function.* The inverse problem of a nonlinear RTM is based on the  
657 minimization of a cost function concurrently measuring the discrepancy between (i) ob-  
658 served and simulated reflectance, and (ii) variables to estimate and the associated prior  
659 information (Jacquemoud et al, 2009b). To avoid solutions reaching fixed boundaries, a  
660 modified cost function in the LUT search that takes uncertainty of provided prior infor-  
661 mation into account is sometimes used, e.g. by means of the above-mentioned Bayesian  
662 approach. Alternatively, Leonenko et al (2013) proposed and evaluated over 60 different  
663 cost functions dealing with different error distributions. Some more spectroscopic stud-  
664 ies have evaluated among others the role of cost function (Danner et al, 2017; Locherer  
665 et al, 2015) in LUT-based inversion. Although the classical RMSE is a robust cost func-  
666 tion, sometimes improvements can be gained with alternative cost functions, e.g. when  
667 the LUTs are non-normal distributed.
  - 668 – The use of *multiple best solutions* in the inversion (mean or median), as opposed to a  
669 single best solution (Banskota et al, 2015; Kattenborn et al, 2017; Koetz et al, 2005;  
670 Locherer et al, 2015).
  - 671 – The addition of *artificial noise* (additive or inverse multiplicative white noise) to account  
672 for uncertainties linked to measurements and models (Danner et al, 2017; Koetz et al,  
673 2005; Locherer et al, 2015).
  - 674 – Several spectroscopic studies reported that the relationship between measured and esti-  
675 mated variable perceptibly improves when only specific (sensitive) spectral ranges are  
676 selected for model inversion (Darvishzadeh et al, 2012; Meroni et al, 2004; Schlerf et al,  
677 2005). To account for noise in the observations, other spectroscopic studies instead ma-  
678 nipulated the observed spectra by applying a smoothing filter (Arellano et al, 2017) or  
679 wavelet transforms (Ali et al, 2016; Banskota et al, 2013; Kattenborn et al, 2017). Spect-  
680 ral selection and spectral polishing methods can be applied at the same time in order to  
681 enhance the resemblance with the usually more spectrally smooth simulated spectra.

682 Because of taking sun-target-sensor geometry into account, the use of RTM-based methods  
683 has been demonstrated to improve robustness to solar and view angle effects, compared to  
684 index-based methods (Kempeneers et al, 2008). Another advantage of RTM inversion rou-  
685 tines is that uncertainties are provided as spectral residuals (Rivera et al, 2013) or standard  
686 deviations, when mapping multiple solution means (Verrelst et al, 2014). Yet the main draw-  
687 back lies in its computational burden resulting from too many per-pixel iterations. Although  
688 LUT-inversion approaches may speed-up the inversion process as opposed to numerical in-  
689 version, these inversion routines are still computationally expensive due to the iterative calls  
690 of LUT entries on a per-pixel basis. Consequently, despite attempts to optimize inversion al-  
691 gorithms in order to save-up computational time for solving inverse radiative transfer prob-  
692 lems (Favennec et al, 2016; Gastellu-Etchegorry et al, 2003), in terms of processing speed  
693 the RTM inversion routines run still behind statistical methods.

## 694 5 Hybrid regression methods

695 Having discussed the more fundamental categories of retrieval methods, this section ad-  
696 dresses *hybrid* regression methods. Hybrid methods combine the generalization level of  
697 physically-based methods with the flexibility and computational efficiency of advanced ma-  
698 chine learning methods. This approach replaces the ground data needed for training of the

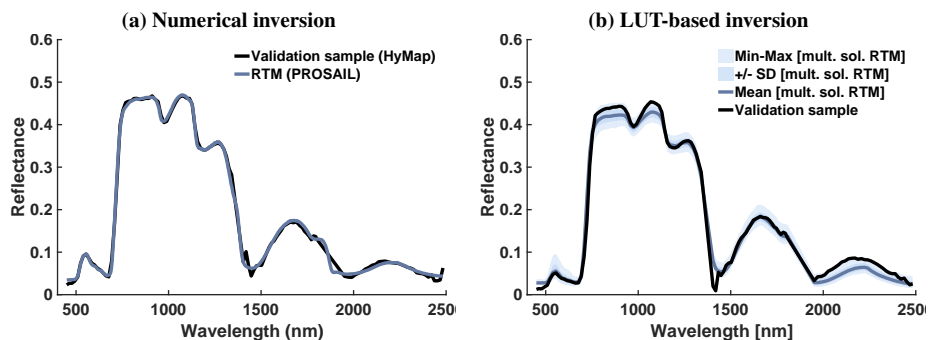


**Fig. 7** Examples of numerical inversion (a) and LUT-based inversion (b). A HyMaP spectrum was inverted against PROSAIL. In case of LUT-inversion, overview statistics of 5% best multiple solutions are shown.

699 parametric or non-parametric models by RTM input variables, which makes it computationally  
 700 efficient. It is important to note that the hybrid approach does not alleviate the main  
 701 issues of RTMs, notably that they only include existing knowledge and concepts. Similarly  
 702 as in case of LUT-based inversion, RTM simulations build a LUT representing a broad set  
 703 of canopy realizations and the hybrid approach uses all available data stored in LUT to train  
 704 a machine learning regression model.

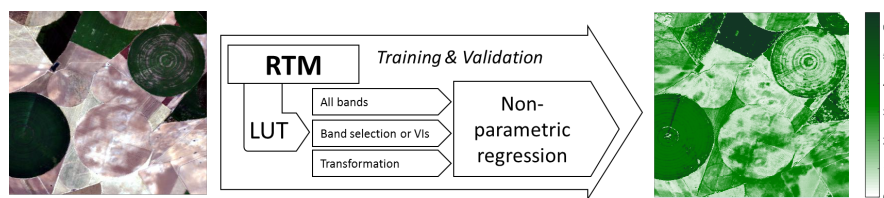


**Fig. 8** Principles of hybrid regression. Left: RGB subset of a hyperspectral HyMaP image (125 bands) over Barrax agricultural site (Spain). Right: illustrative map of a vegetation property (LAI,  $m^2/m^2$ ) as obtained by PROSAIL with Gaussian processes regression (GPR) and 15% white noise added. The model was validated with a  $R^2$  of 0.88 (RMSE: 0.70; NRMSE: 10.1%)

. It took 6.3 seconds to produce the map using ARTMO's MLRA toolbox (Rivera Caicedo et al, 2014). With GPR also uncertainty estimates are provided (not shown). Because not being trained with bare soil spectra, LAI over the non-irrigated parcels is overestimated.

705 The awareness in the mid 90's that ANNs are excellent algorithms to deal with large datasets  
 706 led to the introduction of hybrid methods based on ANNs trained with generically applicable  
 707 RTM-generated data. It led to operational retrieval algorithms for datastreams acquired by  
 708 multispectral and superspectral sensors (see Verrelst et al (2015)). Although this approach  
 709 is less straightforward in the context of imaging spectroscopy, because of the challenge  
 710 of collinearity, some recent efforts have been undertaken in exploring this research direc-  
 711 tion. Noteworthy is the work of Vohland et al (2010) comparing a numerically optimized  
 712 ANN with a LUT-based inversion using PROSAIL RTM simulations. Prediction accura-  
 713 cies generally decreased in the following sequence: numerical optimization > LUT > ANN.  
 714 This would indicate that an ANN may not always be the best choice for inversion applica-  
 715 tions. However, no dimensionality reduction method was applied, which suggests that the  
 716 regression model suffered from band collinearity effects. Also Fei et al (2012) compared  
 717 a PROSAIL-ANN hybrid approach with a PCA approach. The authors concluded that a  
 718 PCA transformation into a regression function can mitigate the known reflectance satura-

tion effect of dense canopies to some extent. This PROSAIL-ANN strategy was revisited by [Rivera-Caicedo et al \(2017\)](#) with alternative dimensionality reduction methods. Although PCA improved accuracies as opposed of using all bands, substantially more improvements were achieved when converting the spectra into components by means canonical correlation analysis (CCA) or orthonormalized PLS (OPLS).

Likewise, inputs from more advanced RTMs were explored to develop specialized hybrid structures. In [Malenovský et al \(2013\)](#) an ANN was trained based on PROSPECT-DART simulations that explicitly took 3D canopy structures into account to estimate forest leaf chlorophyll content from hyperspectral airborne AISA data. In this approach the DART simulations went first through a continuum removal transformation. Alternatively, some studies have attempted to move away from ANN models by exploring hybrid structures on the basis of kernel-based machine learning regression algorithms, particularly the popular SVR. For instance, leaf chlorophyll content was estimated based on a PROSAIL-SVR model and applied to imaging spectroscopy ([Preidl and Doktor, 2011](#)). An analogous concept was applied for a SVR that was trained by PROSPECT-DART simulations in combination with continuum removal transformations, with the purpose of quantifying forest biochemical and structural properties ([Homolová et al, 2016](#)). Similarly, [Doktor et al \(2014\)](#) used a PROSAIL dataset to train a random forests (RF) model to predict LAI and leaf chlorophyll content, and [Liang et al \(2016\)](#) compared PROSAIL-based hybrid models with SVR and RF for leaf and canopy chlorophyll content estimation from CHRIS data. Finally, ([Rivera-Caicedo et al, 2017](#)) analyzed ensembles of regression algorithms with dimensionality reduction methods to consolidate the most ideal PROSAIL-based (2101 bands) hybrid regression model. This study concluded that compressing PROSAIL data into CCA or OPLS components led to highest accuracies when trained with a GPR model. Altogether, although these studies have only been developed in experimental settings – similar as the operational multispectral hybrid algorithms (e.g. [Bacour et al, 2006](#); [Baret et al, 2013](#)) – the hybrid structures can be perfectly implemented into global mapping schemes. When combined with a dimensionality reduction method to suppress collinearity, hybrid methods have a great potential to advance towards operational spectroscopy-based processing schemes.

## 6 Discussion

The mapping of spatially continuous biophysical variables from imaging spectroscopy data is a progressively expanding field of research and development thanks to advances in spectrometer technology and in specialized methods interpreting the acquired spectral data. As a follow-up of an earlier, more general review on retrieval methods applicable to optical remote sensing ([Verrelst et al, 2015](#)), here a summary on retrieval methods specifically applied to spectroscopic data has been compiled. Four categories have been summarized: (1) parametric, (2) non-parametric, (3) RTM inversion, and (4) hybrid methods. The first two categories are statistical methods commonly used with experimental (field) data, whereas the latter two rely on RTM simulations. A schematic flowchart of the main retrieval methods and their hierarchy is provided in [Figure 9](#).

While pros and cons of each of these methodological categories have been earlier discussed ([Verrelst et al, 2015](#)), here we discuss these categories from the perspective of forthcoming routinely-acquired and standardized (e.g., atmospherically-corrected) imaging spectroscopy data streams. First of all, the choice of a method bears implications; not only on the retrievability and processing time of mappable vegetation properties, but also on the purpose of the retrieval. Parametric and non-parametric methods rely on ground data for training, which obviously need to be available in order to apply these methods. If they are available,

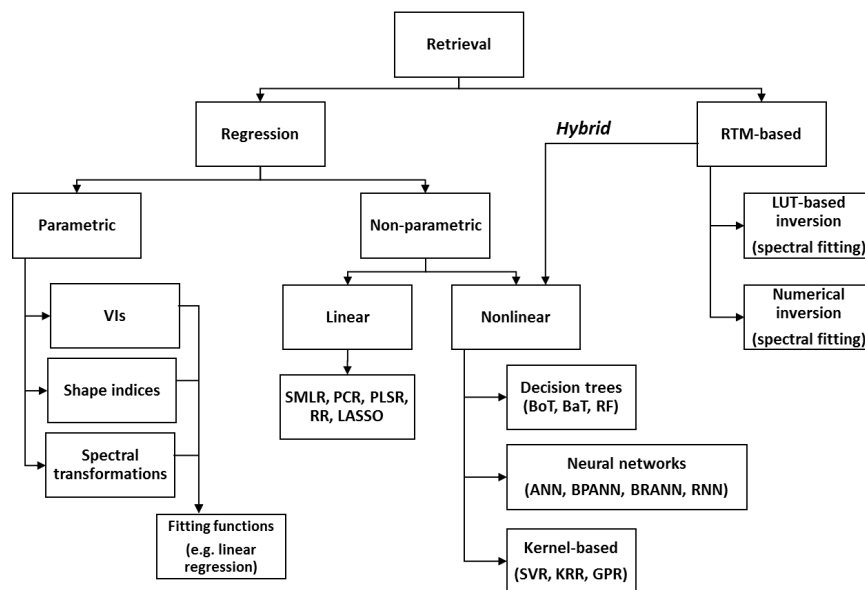


Fig. 9 Schematic overview main retrieval methods.

766 they are the 'shortest' way to the variables of interest, because especially the non-parametric  
 767 methods do not impose any limitation on the relationship between the spectrum and the variable of interest. In contrast, RTMs describe radiative transfer processes, i.e. they use existing  
 768 knowledge (as materialized in the models) rather than ground measured data. Retrieval from  
 769 an RTM through inversion is most useful if one is more interested in the underlying radiative  
 770 transfer processes (scattering, sun- and shade foliage fractions, light distribution within vegetation  
 771 canopies, relationships between canopy structure and photosynthesis), rather than in  
 772 merely extracting a specific variable. However, strategies relying on RTM simulations are  
 773 inherently limited by the input variables of the RTM and, as discussed in section 4, ancillary  
 774 data and regularization methods may be required to optimize their inversions.  
 775

776 Statistical approaches, on the other hand, possess the flexibility to relate reflectance data  
 777 with any measured biophysical variable – state variable or not. As has been demonstrated in  
 778 sections 2 and 3, this can be any quantifiable attribute, typically in the domains of leaf biochemical  
 779 constituents (e.g., nitrogen, phosphorus), pigments (e.g., chlorophyll, carotenoids,  
 780 xanthophylls) or higher-level structural variables (e.g., above-ground biomass, grain yield).  
 781 The strength of the correlation with validation data typically determines the validity and  
 782 transferrability of the statistical model. While this 'seeking for best correlations' can be  
 783 criticized, because of the absence of a physical basis (Knyazikhin et al, 2013), statistical  
 784 approaches are becoming increasingly powerful to extract biochemical variables through  
 785 complex and often indirect relationships. Particularly, machine learning models are powerful  
 786 in extracting information from subtle variations in spectroscopic data through adaptive,  
 787 nonlinear relationships. The advantage of these statistical models is that not only variable-  
 788 specific absorption features can be used for information extraction, but also secondary relationships  
 789 with variables related to other absorption features that co-vary with the variable of  
 790 interest can be exploited (Ollinger, 2011; Verrelst et al, 2012b). Since high accuracies are  
 791 often obtained with these methods, they are gaining popularity, not only for quantification of

792 a diversity of vegetation properties, but also in mapping of floristic composition (Feilhauer  
793 et al, 2017; Harris et al, 2015; Neumann et al, 2016; Roth et al, 2015).

794 Regardless of the nature of retrieval method, in view of mapping larger areas, and especially  
795 in an operational and global context, what matters is the possibility to provide associated  
796 information on the retrieval quality. The characterization of uncertainty is a fundamental  
797 requirement for postulating correct scientific conclusions from results and for assimilating  
798 results into statistical or mechanistic higher-level models (Cressie et al, 2009). As addressed  
799 in section 2, parametric regression methods, i.e. spectral transformation methods in combi-  
800 nation with a fitting function, do not provide uncertainty estimates, which undermine their  
801 applicability to other images in space and time. Subsequently, while valid when locally cal-  
802 ibrated and validated, parametric methods are of little use in an operational context. With  
803 regard to inversion routines, uncertainties can be provided as spectral residuals (Rivera et al,  
804 2013) or standard deviations when mapping multiple solution means (Verrelst et al, 2014).  
805 Lately, inversion approaches were proposed in a Bayesian framework (Shiklomanov et al,  
806 2016), whereby uncertainties are delivered along with the retrievals. In case of traditional  
807 statistical models, uncertainty estimation has been a complex exercise. Statistical models de-  
808 veloped within a Bayesian framework, such as GPR, provide uncertainties together with the  
809 predictions (Camps-Valls et al, 2016; Verrelst et al, 2013b), which indicate the probability  
810 interval of an estimation relative to the samples used during the training phase. These un-  
811 certainties can be used to evaluate GPR model transferability. For example, by mapping the  
812 uncertainties (Verrelst et al, 2013b) demonstrated that a locally developed regression model  
813 can be successfully transported to other images in space and time for the large majority  
814 of pixels (i.e., the uncertainty maps were not systematically worse). Similarly, uncertainties  
815 can inform about the model performance. It was demonstrated that dimensionality reduction  
816 methods applied in GPR models for LAI mapping not only largely sped up the processing,  
817 but they also led to lower per-pixel uncertainties as opposed to mapping using all bands  
818 (Rivera-Caicedo et al, 2017). **In conclusion, in the view of an operational processing need,  
819 just as important as the variable retrieval itself is the provision of an associated uncertainty  
820 estimate. Uncertainty estimates allow evaluating the method's per-pixel performance, and  
821 consequently allow evaluating the method's capability to process routinely acquired imag-  
822 ing data. They thus provide a measure of the retrieval fidelity, which can be used to identify  
823 and mask out the highly uncertain and non-reliable results.**

824 Another important aspect for operational production **of vegetation properties from typically**  
825 **bulky imaging spectroscopy data streams** implies computational speed. Generally, the lower  
826 the complexity of a model the faster it will be able to produce maps. This highly favors  
827 the application of parametric regression approaches since they consist of only few trans-  
828 formations and equations. Also non-parametric regression algorithms, once trained, can be  
829 applied to process an images almost instantaneously. Training of machine learning mod-  
830 els is frequently related to the tuning of several free variables with costly cross-validation  
831 approaches. These scale poorly with the number of samples (such as in kernel machines)  
832 or with the data dimensions (such as in ANNs). Although a trained ANN converts an im-  
833 age into a map quasi-instantly, kernel-based methods require more processing time, be-  
834 cause the similarity between each test pixel in the image and those used to train the model  
835 has to be estimated. Training can be computationally costly, especially when using a big  
836 training dataset, e.g. as in hybrid strategies. A solution to shorten training time could be in  
837 size reduction of the training data in a way that maximal relevant information is preserved.  
838 This can be achieved by means of dimensionality reduction methods in the spectral domain  
839 (Rivera-Caicedo et al, 2017), or by means of intelligent sampling in the sampling domain,  
840 e.g. through active learning (Verrelst et al, 2016a).

841 Considerably longer run-time is expected in case of inversion routines. Since RTMs take  
842 some time to generate simulations, especially for computationally expensive models, and  
843 also the evaluation takes place on a per-pixel basis, the iterative inversion routines are com-  
844 putationally expensive leading to relatively slow mapping speeds. In an attempt to accel-  
845 erate their mapping speed, it has been proposed to approximate the functioning of the original  
846 RTM by means of statistical learning called *emulation* (Gómez-Dans et al, 2016; Rivera  
847 et al, 2015). Initial experiments to emulate leaf, canopy and atmospheric RTMs demon-  
848 strated that emulators can successfully generate spectral output from a limited set of input  
849 variable almost instantly, thereby preserving sufficient accuracy as compared to the origi-  
850 nal RTM (Verrelst et al, 2016c, 2017). Although an emulator reproduces RTM simulations  
851 instantly, application of a per-pixel spectral fitting requires many repetitions, which implies  
852 that these methods still do not reach the speed of statistical methods.

853 All in all, having the purpose of advancing towards operational imaging spectroscopy data  
854 processing in mind, i.e., reaching globally-applicable, accurate and fast estimates, we end  
855 up with the following recommendations:

- 856 – To enable model transferability to routinely-acquired images, retrieval methods must  
857 provide associated per-pixel uncertainties as a quality indicator whether the model can  
858 perform adequately in another space and time.
- 859 – Regarding the computational speed, e.g. in case of repetitive image processing, statisti-  
860 cal (i.e. regression) methods are multiple times faster than physically-based methods,  
861 capable to process full images in the order of minutes or even seconds.
- 862 – In case of regression methods (experimental or hybrid), multicollinearity of spectro-  
863 scopic data complicates the development of powerful models. Physically-based methods  
864 using spectral fitting do not suffer from this problem.
- 865 – To mitigate the problem of multicollinearity in regression methods, either band selec-  
866 tion or dimensionality reduction methods can be applied before entering the regression.  
867 Although band selection is a common practice, likely more powerful regression models  
868 can be obtained when using a dimensionality reduction method.

## 869 7 Conclusions

870 With forthcoming imaging spectrometer satellite missions, an unprecedented stream of datasets  
871 on the terrestrial biosphere will become available. This will require powerful processing  
872 techniques enabling quantification of vegetation variables in an operational and global set-  
873 ting. Four categories of retrieval methods have been discussed in this review paper: (1) para-  
874 metric regression; (2) non-parametric regression; (3) physically-based RTM inversion; and,  
875 (4) hybrid methods. For each of these categories, a diversity of methodological approaches  
876 are increasingly applied to imaging spectroscopy data. This literature review synthesized the  
877 current state-of-the-art in the field of spectroscopy-based vegetation properties mapping.

878 Although parametric methods, such as shape indices or spectral transformation, deal well  
879 with extracting relevant information embedded in spectroscopic data, their lack of uncer-  
880 tainty estimates makes them unsuitable for operational use. Higher accuracies can be reached  
881 with nonlinear non-parametric methods; especially those in the field of machine learning that  
882 generate probabilistic outputs, e.g. Gaussian process regression. However, an additional step  
883 to mitigate their spectral multicollinearity is deemed necessary. A popular strategy in this  
884 respect is selecting a set of vegetation indices or applying spectral transformation before  
885 training the machine learning algorithm. It remains nevertheless questionable whether such  
886 band selection approaches fully capture all relevant information. Instead, dimensionality re-



887 duction methods that enable compressing the large majority of spectral variability into a few  
888 components tend to lead to more accurate predictions.

889 On the other hand, the inversion of physically-based RTMs against spectroscopic data is  
890 generally applicable and physically sound, but optimizing their inversion strategies is more  
891 challenging compared to the regression methods. RTM-based inversion is computationally  
892 demanding and ancillary information is usually required as an input or to regulate the in-  
893 version algorithm. Hybrid regression methods, based on the coupling of an RTM with a  
894 machine learning regression algorithm, overcome the problem of processing speed. Particu-  
895 larly Bayesian kernel-based hybrid strategies possess promising features, as they combine  
896 speed, flexibility and the provision of uncertainty estimates. Their accuracies and processing  
897 speed can be further improved in combination with dimensionality reduction. Altogether,  
898 and in the interest of operational spectroscopy-based mapping of vegetation properties, we  
899 recommend to further explore the feasibility and implementation of hybrid strategies into  
900 the next-generation data processing chains.

## 901 References

- 902 Adam E, Mutanga O, Abdel-Rahman E, Ismail R (2014) Estimating standing biomass in  
903 papyrus (*Cyperus papyrus* L.) swamp: Exploratory of in situ hyperspectral indices and  
904 random forest regression. *International Journal of Remote Sensing* 35(2):693–714
- 905 Addink E, De Jong S, Pebesma E (2007) The importance of scale in object-based mapping  
906 of vegetation parameters with hyperspectral imagery. *Photogrammetric Engineering and*  
907 *Remote Sensing* 73(8):905–912
- 908 Ali A, Skidmore A, Darvishzadeh R, van Duren I, Holzwarth S, Mueller J (2016) Retrieval  
909 of forest leaf functional traits from HySpex imagery using radiative transfer models and  
910 continuous wavelet analysis. *ISPRS Journal of Photogrammetry and Remote Sensing*  
911 122:68–80
- 912 Alton P, Ellis R, Los S, North P (2007) Improved global simulations of gross primary prod-  
913 uct based on a separate and explicit treatment of diffuse and direct sunlight. *Journal of*  
914 *Geophysical Research: Atmospheres* 112(D7)
- 915 Arellano P, Tansey K, Balzter H, Tellkamp M (2017) Plant family-specific impacts of  
916 petroleum pollution on biodiversity and leaf chlorophyll content in the Amazon rainforest  
917 of Ecuador. *PLoS ONE* 12(1)
- 918 Arenas-García J, Camps-Valls G (2008) Efficient kernel orthonormalized PLS for re-  
919 mote sensing applications. *IEEE Transactions on Geoscience and Remote Sensing*  
920 46(10):2872–2881
- 921 Ashourloo D, Aghighi H, Matkan A, Mobasheri M, Rad A (2016) An investigation into  
922 machine learning regression techniques for the leaf rust disease detection using hyper-  
923 spectral measurement. *IEEE Journal of Selected Topics in Applied Earth Observations*  
924 *and Remote Sensing* 9(9):4344–4351
- 925 Atzberger C, Guérif M, Baret F, Werner W (2010) Comparative analysis of three chemo-  
926 metric techniques for the spectroradiometric assessment of canopy chlorophyll content in  
927 winter wheat. *Computers and Electronics in Agriculture* 73(2):165–173
- 928 Atzberger C, Darvishzadeh R, Immitzer M, Schlerf M, Skidmore A, le Maire G (2015)  
929 Comparative analysis of different retrieval methods for mapping grassland leaf area index  
930 using airborne imaging spectroscopy. *International Journal of Applied Earth Observation*  
931 *and Geoinformation* 43:19–31

- 932 Bacour C, Baret F, Béal D, Weiss M, Pavageau K (2006) Neural network estimation of LAI,  
933 fAPAR, fCover and LAI×Cab, from top of canopy MERIS reflectance data: Principles  
934 and validation. *Remote Sensing of Environment* 105(4):313–325
- 935 Balzarolo M, Vescovo L, Hammerle A, Gianelle D, Papale D, Tomelleri E, Wohlfahrt G  
936 (2015) On the relationship between ecosystem-scale hyperspectral reflectance and CO<sub>2</sub>  
937 exchange in European mountain grasslands. *Biogeosciences* 12(10):3089–3108
- 938 Banskota A, Wynne R, Thomas V, Serbin S, Kayastha N, Gastellu-Etchegorry J, Townsend P  
939 (2013) Investigating the utility of wavelet transforms for inverting a 3-D radiative transfer  
940 model using hyperspectral data to retrieve forest LAI. *Remote Sensing* 5(6):2639–2659
- 941 Banskota A, Serbin S, Wynne R, Thomas V, Falkowski M, Kayastha N, Gastellu-Etchegorry  
942 JP, Townsend P (2015) An LUT-Based Inversion of DART Model to Estimate Forest LAI  
943 from Hyperspectral Data. *IEEE Journal of Selected Topics in Applied Earth Observations  
944 and Remote Sensing* 8(6):3147–3160
- 945 Bao S, Cao C, Chen W, Tian H (2017) Spectral features and separability of alpine wetland  
946 grass species. *Spectroscopy Letters* 50(5):245–256
- 947 Baranoski G, Rokne J (2005) A practical approach for estimating the red edge position of  
948 plant leaf reflectance. *International Journal of Remote Sensing* 26(3):503–521
- 949 Baret F, Buis S (2008) Estimating canopy characteristics from remote sensing observations.  
950 Review of methods and associated problems. In S Liang (Ed), *Advances in Land Remote  
951 Sensing: System, Modeling, Inversion and Application*, Springer pp 171–200
- 952 Baret F, Weiss M, Lacaze R, Camacho F, Makhmara H, Pacholczyk P, Smets B (2013)  
953 GEOV1: LAI and FAPAR essential climate variables and FCOVER global time series  
954 capitalizing over existing products. Part1: Principles of development and production .  
955 *Remote Sensing of Environment* 137(0):299 – 309
- 956 Barton CVM, North P (2001) Remote sensing of canopy light use efficiency using the pho-  
957 tochemical reflectance index: Model and sensitivity analysis. *Remote Sensing of Envi-  
958 ronment* 78(3):264–273
- 959 Bayat B, van der Tol C, Verhoef W (2016) Remote sensing of grass response to drought  
960 stress using spectroscopic techniques and canopy reflectance model inversion. *Remote  
961 Sensing* 8(7)
- 962 Belgiu M, Drăguț L (2016) Random forest in remote sensing: A review of applications and  
963 future directions. *ISPRS Journal of Photogrammetry and Remote Sensing* 114:24–31
- 964 Berk A, Anderson G, Acharya P, Bernstein L, Muratov L, Lee J, Fox M, Adler-Golden S,  
965 Chetwynd J, Hoke M, Lockwood R, Gardner J, Cooley T, Borel C, Lewis P, Shettle E  
966 (2006) MODTRAN<sup>TM</sup>5: 2006 update. vol 6233 II
- 967 Botha E, Leblon B, Zebarth B, Watmough J (2007) Non-destructive estimation of potato leaf  
968 chlorophyll from canopy hyperspectral reflectance using the inverted PROSAIL model.  
969 *International Journal of Applied Earth Observation and Geoinformation* 9(4):360–374
- 970 Bratsch S, Epstein H, Buchhorn M, Walker D, Landes H (2017) Relationships between hy-  
971 perspectral data and components of vegetation biomass in Low Arctic tundra communities  
972 at Ivotuk, Alaska. *Environmental Research Letters* 12(2)
- 973 Breiman L (1996) Bagging predictors. *Machine Learning* 24(2):123–140
- 974 Breiman L (2001) Random forests. *Machine Learning* 45(1):5–32
- 975 Breiman L, Friedman J, Stone C, Olshen R (1984) *Classification and Regression Trees*. The  
976 Wadsworth and Brooks-Cole statistics-probability series, Taylor & Francis
- 977 Broge NH, Leblanc E (2001) Comparing prediction power and stability of broadband and  
978 hyperspectral vegetation indices for estimation of green leaf area index and canopy  
979 chlorophyll density. *Remote Sensing of Environment* 76(2):156–172
- 980 Broomhead DS, Lowe D (1988) Radial basis functions, multi-variable functional interpola-  
981 tion and adaptive networks. Tech. rep., Royal Signals and Radar Establishment Malvern

- 982 (United Kingdom)
- 983 Buchhorn M, Walker DA, Heim B, Raynolds MK, Epstein HE, Schwieder M (2013)
- 984 Ground-based hyperspectral characterization of alaska tundra vegetation along environ-
- 985 mental gradients. *Remote Sensing* 5(8):3971–4005
- 986 Burden F, Winkler D (1999) Robust QSAR models using bayesian regularized neural net-
- 987 works. *Journal of Medicinal Chemistry* 42(16):3183–3187
- 988 Bye I, North P, Los S, Kljun N, Rosette J, Hopkinson C, Chasmer L, Mahoney C (2017) Es-
- 989 timating forest canopy parameters from satellite waveform LiDAR by inversion of the
- 990 FLIGHT three-dimensional radiative transfer model. *Remote Sensing of Environment*
- 991 188:177–189
- 992 Camps-Valls G, Verrelst J, Muñoz-Marí J, Laparra V, Mateo-Jiménez F, Gómez-Dans J
- 993 (2016) A survey on Gaussian processes for earth observation data analysis. *IEEE Geo-*
- 994 *science and Remote Sensing Magazine* 4(2)
- 995 Capolupo A, Kooistra L, Berendonk C, Boccia L, Suomalainen J (2015) Estimating plant
- 996 traits of grasslands from UAV-acquired hyperspectral images: A comparison of statistical
- 997 approaches. *ISPRS International Journal of Geo-Information* 4(4):2792–2820
- 998 Chen B, Wu Z, Wang J, Dong J, Guan L, Chen J, Yang K, Xie G (2015) Spatio-temporal pre-
- 999 diction of leaf area index of rubber plantation using HJ-1A/1B CCD images and recurrent
- 1000 neural network. *ISPRS Journal of Photogrammetry and Remote Sensing* 102:148–160
- 1001 Cho MA, Skidmore AK (2006) A new technique for extracting the red edge position from
- 1002 hyperspectral data: The linear extrapolation method. *Remote sensing of environment*
- 1003 101(2):181–193
- 1004 Cho MA, Skidmore AK, Atzberger C (2008) Towards red-edge positions less sensitive to
- 1005 canopy biophysical parameters for leaf chlorophyll estimation using properties optique
- 1006 spectrales des feuilles (PROSPECT) and scattering by arbitrarily inclined leaves (SAILH)
- 1007 simulated data. *International Journal of Remote Sensing* 29(8):2241–2255
- 1008 Cho Mb, Skidmore Ab, Corsi F, van Wieren S, Sobhan Ib (2007) Estimation of green
- 1009 grass/herb biomass from airborne hyperspectral imagery using spectral indices and partial
- 1010 least squares regression. *International Journal of Applied Earth Observation and Geoin-*
- 1011 *formation* 9(4):414–424
- 1012 Clark RN, Roush TL (1984) Reflectance spectroscopy: Quantitative analysis techniques for
- 1013 remote sensing applications. *Journal of Geophysical Research: Solid Earth* 89(B7):6329–
- 1014 6340
- 1015 Clevers J (2014) Beyond NDVI: Extraction of biophysical variables from remote sensing
- 1016 imagery. *Remote Sensing and Digital Image Processing* 18:363–381
- 1017 Clevers J, Kooistra L (2012) Using hyperspectral remote sensing data for retrieving canopy
- 1018 chlorophyll and nitrogen content. *IEEE Journal of Selected Topics in Applied Earth Ob-*
- 1019 *servations and Remote Sensing* 5(2):574–583
- 1020 Clevers JGPW, Kooistra L, Salas EAL (2004) Study of heavy metal contamination in river
- 1021 floodplains using the red-edge position in spectroscopic data. *International Journal of*
- 1022 *Remote Sensing* 25(19):3883–3895
- 1023 Coops NC, Smith ML, Martin M, Ollinger SV (2003) Prediction of eucalypt foliage nitrogen
- 1024 content from satellite-derived hyperspectral data. *IEEE Transactions on Geoscience and*
- 1025 *Remote Sensing* 41(6):1338–1346
- 1026 Cressie N, Calder C, Clark J, Ver Hoef J, Wikle C (2009) Accounting for uncertainty in eco-
- 1027 logical analysis: The strengths and limitations of hierarchical statistical modeling. *Eco-*
- 1028 *logical Applications* 19(3):553–570
- 1029 Danner M, Berger K, Wocher M, Mauser W, Hank T (2017) Retrieval of biophysical crop
- 1030 variables from multi-angular canopy spectroscopy. *Remote Sensing* 9(7)

- 1031 Darvishzadeh R, Skidmore A, Schlerf M, Atzberger C (2008) Inversion of a radiative transfer model for estimating vegetation LAI and chlorophyll in a heterogeneous grassland. Remote Sensing of Environment 112(5):2592–2604
- 1032  
1033
- 1034 Darvishzadeh R, Matkan AA, Dashti Ahangar A (2012) Inversion of a radiative transfer model for estimation of rice canopy chlorophyll content using a lookup-table approach. IEEE Journal of Selected Topics in Applied Earth Observations and Remote Sensing PP(99):1–9
- 1035  
1036  
1037
- 1038 Dawson T, Curran P, Plummer S (1998) LIBERTY - Modeling the effects of Leaf Biochemical Concentration on Reflectance Spectra. Remote Sensing of Environment 65(1):50–60
- 1039  
1040 Delegido J, Alonso L, González G, Moreno J (2010) Estimating chlorophyll content of crops from hyperspectral data using a normalized area over reflectance curve (NAOC). International Journal of Applied Earth Observation and Geoinformation 12(3):165–174
- 1041  
1042 Delegido J, Verrelst J, Alonso L, Moreno J (2011) Evaluation of sentinel-2 red-edge bands for empirical estimation of green LAI and chlorophyll content. Sensors 11(7):7063–7081
- 1043  
1044 Delegido J, Verrelst J, Meza C, Rivera J, Alonso L, Moreno J (2013) A red-edge spectral index for remote sensing estimation of green LAI over agroecosystems. European Journal of Agronomy 46:42–52
- 1045  
1046  
1047
- 1048 Dietz A, Kuenzer C, Gessner U, Dech S (2012) Remote sensing of snow - a review of available methods. International Journal of Remote Sensing 33(13):4094–4134
- 1049  
1050 Disney M, Lewis P, Saich P (2006) 3D modelling of forest canopy structure for remote sensing simulations in the optical and microwave domains. Remote Sensing of Environment 100(1):114–132
- 1051  
1052
- 1053 Doktor D, Lausch A, Spengler D, Thurner M (2014) Extraction of plant physiological status from hyperspectral signatures using machine learning methods. Remote Sensing 6(12):12,247–12,274
- 1054  
1055
- 1056 Dorigo W, Richter R, Baret F, Bamler R, Wagner W (2009) Enhanced automated canopy characterization from hyperspectral data by a novel two step radiative transfer model inversion approach. Remote Sensing 1(4):1139–1170
- 1057  
1058
- 1059 Dorigo WA, Zurita-Milla R, de Wit AJW, Brazile J, Singh R, Schaepman ME (2007) A review on reflective remote sensing and data assimilation techniques for enhanced agroecosystem modeling. International Journal of Applied Earth Observation and Geoinformation 9(2):165–193
- 1060  
1061  
1062
- 1063 Draper NR, Smith H (2014) Applied regression analysis. John Wiley & Sons
- 1064 Dreccer M, Barnes L, Meder R (2014) Quantitative dynamics of stem water soluble carbohydrates in wheat can be monitored in the field using hyperspectral reflectance. Field Crops Research 159:70–80
- 1065  
1066
- 1067 Drusch M, Moreno J, Del Bello U, Franco R, Goulas Y, Huth A, Kraft S, Middleton EM, Miglietta F, Mohammed G, et al (2017) The FLuorescence EXplorer Mission Concept-ESA's Earth Explorer 8. IEEE Transactions on Geoscience and Remote Sensing 55(3):1273–1284
- 1068  
1069  
1070
- 1071 Du L, Shi S, Yang J, Sun J, Gong W (2016) Using different regression methods to estimate leaf nitrogen content in rice by fusing hyperspectral LiDAR data and laser-induced chlorophyll fluorescence data. Remote Sensing 8(6)
- 1072  
1073
- 1074 Duan SB, Li ZL, Wu H, Tang BH, Ma L, Zhao E, Li C (2014) Inversion of the prosail model to estimate leaf area index of maize, potato, and sunflower fields from unmanned aerial vehicle hyperspectral data. International Journal of Applied Earth Observation and Geoinformation 26(1):12–20
- 1075  
1076  
1077
- 1078 Elvidge CD, Chen Z (1995) Comparison of broad-band and narrow-band red and near-infrared vegetation indices. Remote Sensing of Environment 54(1):38–48
- 1079

- 1080 Favennec Y, Le Hardy D, Dubot F, Rousseau B, Rouse D (2016) Some speed-up strategies  
1081 for solving inverse radiative transfer problems. *Journal of Physics: Conference Series*  
1082 676(1)
- 1083 Fei Y, Jiulin S, Hongliang F, Zuofang Y, Jiahua Z, Yunqiang Z, Kaishan S, Zongming W,  
1084 Maogui H (2012) Comparison of different methods for corn LAI estimation over north-  
1085 eastern China. *International Journal of Applied Earth Observation and Geoinformation*  
1086 18:462–471
- 1087 Feilhauer H, Asner GP, Martin RE (2015) Multi-method ensemble selection of spectral  
1088 bands related to leaf biochemistry. *Remote Sensing of Environment* 164:57 – 65
- 1089 Feilhauer H, Somers B, van der Linden S (2017) Optical trait indicators for remote sens-  
1090 ing of plant species composition: Predictive power and seasonal variability. *Ecological*  
1091 *Indicators* 73:825–833
- 1092 Feng H, Yang F, Li Z, Yang G, Guo J, He P, Wang Y (2016) Hyperspectral estimation of  
1093 leaf total phosphorus content in apple tree based on optimal weights combination model.  
1094 *Nongye Gongcheng Xuebao/Transactions of the Chinese Society of Agricultural Engi-  
1095 neering* 32(7):173–180
- 1096 Feret JB, François C, Asner GP, Gitelson AA, Martin RE, Bidet LPR, Ustin SL, le Maire G,  
1097 Jacquemoud S (2008) PROSPECT-4 and 5: Advances in the leaf optical properties model  
1098 separating photosynthetic pigments. *Remote Sensing of Environment* 112(6):3030–3043
- 1099 Foster A, Kakani V, Mosali J (2017) Estimation of bioenergy crop yield and N status by  
1100 hyperspectral canopy reflectance and partial least square regression. *Precision Agriculture*  
1101 18(2):192–209
- 1102 Franci L, Panigrahi S (1997) Artificial neural network models of wheat leaf wetness. *Agricul-  
1103 tural and Forest Meteorology* 88(1-4):57–65
- 1104 Friedman J, Hastie T, Tibshirani R (2000) Additive logistic regression: A statistical view of  
1105 boosting. *Annals of Statistics* 28(2):337–407
- 1106 Fu Y, Yang G, Feng H, Xu X, Song X, Wang J (2012) Comparison of winter wheat LAI es-  
1107 timation methods based on hyperspectral dimensionality reduction and vegetation index.  
1108 *Nongye Gongcheng Xuebao/Transactions of the Chinese Society of Agricultural Engi-  
1109 neering* 28(23):107–113
- 1110 Gastellu-Etchegorry J, Demarez V, Pinel V, Zagolski F (1996) Modeling radiative transfer in  
1111 heterogeneous 3-D vegetation canopies. *Remote Sensing of Environment* 58(2):131–156
- 1112 Gastellu-Etchegorry J, Guillevic P, Zagolski F, Demarez V, Trichon V, Deering D, Leroy M  
1113 (1999) Modeling BRDF and radiation regime of boreal and tropical forests: I. BRDF. *Remote*  
1114 *Sensing of Environment* 68(3):281–316
- 1115 Gastellu-Etchegorry J, Gascon F, Esteve P (2003) An interpolation procedure for generaliz-  
1116 ing a look-up table inversion method. *Remote Sensing of Environment* 87(1):55–71
- 1117 Gastellu-Etchegorry J, Martin E, Gascon F (2004) DART: a 3D model for simulating satellite  
1118 images and studying surface radiation budget. *International journal of remote sensing*  
1119 25(1):73–96
- 1120 Gastellu-Etchegorry J, Lauret N, Yin T, Landier L, Kallel A, Malenovský Z, Al Bitar A,  
1121 Aval J, Benhmida S, Qi J, Medjdoub G, Guilleux J, Chavanon E, Cook B, Morton D,  
1122 Nektarios N, Mitraka Z (2017) DART: Recent advances in remote sensing data modeling  
1123 with atmosphere, polarization, and chlorophyll fluorescence. *IEEE Journal of Selected*  
1124 *Topics in Applied Earth Observations and Remote Sensing* p In press (accepted 8 March  
1125 2017)
- 1126 Gastellu-Etchegorry JP, Yin T, Lauret N, Cajgfinger T, Gregoire T, Grau E, Feret JB,  
1127 Lopes M, Guilleux J, Dedieu G, Malenovský Z, Cook B, Morton D, Rubio J, Durrieu S,  
1128 Cazanave G, Martin E, Ristorcelli T (2015) Discrete anisotropic radiative transfer (DART  
1129 5) for modeling airborne and satellite spectroradiometer and LIDAR acquisitions of nat-

- 1130 ural and urban landscapes. *Remote Sensing* 7(2):1667–1701
- 1131 Gastellu-Etchegorry JP, Yin T, Lauret N, Grau E, Rubio J, Cook B, Morton D, Sun G (2016)
- 1132 Simulation of satellite, airborne and terrestrial LiDAR with DART (I): Waveform simula-  
1133 tion with quasi-Monte Carlo ray tracing. *Remote Sensing of Environment* 184:418–435
- 1134 Geladi P, Kowalski B (1986) Partial least-squares regression: a tutorial. *Analytica Chimica*  
1135 *Acta* 185(C):1–17
- 1136 Gwali U, Monteiro S, Saber E (2018) Machine learning based hyperspectral image analy-  
1137 sis: A survey. *ISPRS Journal of Photogrammetry and Remote Sensing* (submitted)
- 1138 Gianelle D, Guastella Fb (2007) Nadir and off-nadir hyperspectral field data: Strengths and  
1139 limitations in estimating grassland biophysical characteristics. *International Journal of*  
1140 *Remote Sensing* 28(7):1547–1560
- 1141 Glenn E, Huete A, Nagler P, Nelson S (2008) Relationship between remotely-sensed vegeta-  
1142 tion indices, canopy attributes and plant physiological processes: What vegetation indices  
1143 can and cannot tell us about the landscape. *Sensors* 8(4):2136–2160
- 1144 Gómez-Chova L, Muñoz-Marí J, Laparra V, Malo-López J, Camps-Valls G (2011) A review  
1145 of kernel methods in remote sensing data analysis. In: *Optical Remote Sensing*, Springer,  
1146 pp 171–206
- 1147 Gómez-Dans JL, Lewis PE, Disney M (2016) Efficient emulation of radiative transfer codes  
1148 using gaussian processes and application to land surface parameter inferences. *Remote*  
1149 *Sensing* 8(2):119
- 1150 Gonsamo A (2011) Normalized sensitivity measures for leaf area index estimation us-  
1151 ing three-band spectral vegetation indices. *International Journal of Remote Sensing*  
1152 32(7):2069–2080
- 1153 Govaerts YM, Verstraete MM (1998) Raytran: A Monte Carlo ray-tracing model to com-  
1154 pute light scattering in three-dimensional heterogeneous media. *IEEE Transactions on*  
1155 *Geoscience and Remote Sensing* 36(2):493–505
- 1156 Grau E, Gastellu-Etchegorry JP (2013) Radiative transfer modeling in the Earth-  
1157 Atmosphere system with DART model. *Remote sensing of environment* 139:149–170
- 1158 Guanter L, Kaufmann H, Segl K, Foerster S, Rogass C, Chabrillat S, Kuester T, Hollstein A,  
1159 Rossner G, Chlebek C, Straif C, Fischer S, Schrader S, Storch T, Heiden U, Mueller A,  
1160 Bachmann M, Muhle H, Muller R, Habermeyer M, Ohndorf A, Hill J, Buddenbaum H,  
1161 Hostert P, van der Linden S, Leitao PJ, Rabe A, Doerffer R, Krasemann H, Xi H, Mauser  
1162 W, Hank T, Locherer M, Rast M, Staenz K, Sang B (2015) The EnMAP Spaceborne  
1163 Imaging Spectroscopy Mission for Earth Observation. *Remote Sensing* 7(7):8830
- 1164 Guillevic P, Gastellu-Etchegorry J, Demarty J, Prévot L (2003) Thermal infrared radiative  
1165 transfer within three-dimensional vegetation covers. *Journal of Geophysical Research:*  
1166 *Atmospheres* 108(D8)
- 1167 Han ZY, Zhu XC, Fang XY, Wang ZY, Wang L, Zhao GX, Jiang YM (2016) Hyperspectral  
1168 estimation of apple tree canopy LAI based on SVM and RF regression. *Guang Pu Xue Yu*  
1169 *Guang Pu Fen Xi/Spectroscopy and Spectral Analysis* 36(3):800–805
- 1170 Hancock S, Lewis P, Foster M, Disney M, Muller JP (2012) Measuring forests with dual  
1171 wavelength lidar: A simulation study over topography. *Agricultural and Forest Meteorol-*  
1172 *ogy* 161:123–133
- 1173 Hansen PM, Schjoerring JK (2003) Reflectance measurement of canopy biomass and nitro-  
1174 gen status in wheat crops using normalized difference vegetation indices and partial least  
1175 squares regression. *Remote Sensing of Environment* 86(4):542–553
- 1176 Harris A, Charnock R, Lucas R (2015) Hyperspectral remote sensing of peatland floristic  
1177 gradients. *Remote Sensing of Environment* 162:99–111
- 1178 Haykin S (1999) *Neural Networks – A Comprehensive Foundation*, 2nd edn. Prentice Hall

- 1179 He R, Qiao X, Jiang J, Guo H (2015) Retrieving canopy leaf total nitrogen content of winter  
1180 wheat by continuous wavelet transform. *Nongye Gongcheng Xuebao/Transactions of the*  
1181 *Chinese Society of Agricultural Engineering* 31(2):141–146
- 1182 Heiskanen J, Rautiainen M, Stenberg P, Möttöus M, Vesanto VH (2013) Sensitivity of nar-  
1183 rowband vegetation indices to boreal forest LAI, reflectance seasonality and species com-  
1184 position. *ISPRS Journal of Photogrammetry and Remote Sensing* 78:1–14
- 1185 Hernández-Clemente R, North P, Hornero A, Zarco-Tejada P (2017) Assessing the effects  
1186 of forest health on sun-induced chlorophyll fluorescence using the FluorFLIGHT 3-D  
1187 radiative transfer model to account for forest structure. *Remote Sensing of Environment*  
1188 193:165–179
- 1189 Hochreiter S, Schmidhuber J (1997) Long short-term memory. *Neural Computation*  
1190 9(8):1735–1780
- 1191 Homolová L, Janoutová R, Malenovský Z (2016) Evaluation of various spectral inputs for  
1192 estimation of forest biochemical and structural properties from airborne imaging spec-  
1193 troscopy data. vol 41, pp 961–966
- 1194 Huang Y, Tian Q, Wang L, Geng J, Lyu C (2014) Estimating canopy leaf area index in  
1195 the late stages of wheat growth using continuous wavelet transform. *Journal of Applied*  
1196 *Remote Sensing* 8(1)
- 1197 Huang Z, Turner BJ, Dury SJ, Wallis IR, Foley WJ (2004) Estimating foliage nitrogen con-  
1198 centration from HYMAP data using continuum removal analysis. *Remote Sensing of En-  
1199 vironment* 93(1):18–29
- 1200 Hughes G (1968) On the mean accuracy of statistical pattern recognizers. *IEEE Transactions*  
1201 *on Information Theory* 14(1):55–63
- 1202 Im J, Jensen JR, Coleman M, Nelson E (2009) Hyperspectral remote sensing analysis of  
1203 short rotation woody crops grown with controlled nutrient and irrigation treatments. *Geo-  
1204 carto International* 24(4):293–312
- 1205 Jacquemoud S, Baret F, Andrieu B, Danson FM, Jaggard K (1995) Extraction of vegeta-  
1206 tion biophysical parameters by inversion of the PROSPECT+SAIL models on sugar beet  
1207 canopy reflectance data. Application to TM and AVIRIS sensors. *Remote Sensing of En-  
1208 vironment* 52(3):163–172
- 1209 Jacquemoud S, Verhoef W, Baret F, Bacour C, Zarco-Tejada P, Asner G, François C, Ustin  
1210 S (2009a) PROSPECT + SAIL models: A review of use for vegetation characterization.  
1211 *Remote Sensing of Environment* 113(SUPPL. 1):S56–S66
- 1212 Jacquemoud S, Verhoef W, Baret F, Bacour C, Zarco-Tejada P, Asner G, François C, Ustin  
1213 S (2009b) PROSPECT + SAIL models: A review of use for vegetation characterization.  
1214 *Remote Sensing of Environment* 113(SUPPL. 1):S56–S66
- 1215 Jay S, Bendoula R, Hadoux X, Féret JB, Gorretta N (2016) A physically-based model for re-  
1216 trieving foliar biochemistry and leaf orientation using close-range imaging spectroscopy.  
1217 *Remote Sensing of Environment* 177:220–236
- 1218 Jensen R, Hardin P, Hardin A (2012) Estimating urban leaf area index (LAI) of individ-  
1219 ual trees with hyperspectral data. *Photogrammetric Engineering and Remote Sensing*  
1220 78(5):495–504
- 1221 Jia F, Liu G, Liu D, Zhang Y, Fan W, Xing X (2013) Comparison of different methods  
1222 for estimating nitrogen concentration in flue-cured tobacco leaves based on hyperspectral  
1223 reflectance. *Field Crops Research* 150:108–114
- 1224 Kalacska M, Lalonde M, Moore T (2015) Estimation of foliar chlorophyll and nitrogen  
1225 content in an ombrotrophic bog from hyperspectral data: Scaling from leaf to image.  
1226 *Remote Sensing of Environment* 169:270–279
- 1227 Kanke Y, Tubaña B, Dalen M, Harrell D (2016) Evaluation of red and red-edge reflectance-  
1228 based vegetation indices for rice biomass and grain yield prediction models in paddy

- 1229 fields. *Precision Agriculture* 17(5):507–530
- 1230 Karimi Y, Prasher S, Madani A, Kim S (2008) Application of support vector machine tech-  
1231 nology for the estimation of crop biophysical parameters using aerial hyperspectral obser-  
1232 vations. *Canadian Biosystems Engineering / Le Genie des biosystems au Canada* 50:7.13–  
1233 7.20
- 1234 Kattenborn T, Fassnacht F, Pierce S, Lopatin J, Grime J, Schmidtlein S (2017) Linking plant  
1235 strategies and plant traits derived by radiative transfer modelling. *Journal of Vegetation*  
1236 *Science* 28(4):717–727
- 1237 Kempeneers P, Zarco-Tejada PJ, North PRJ, de Backer S, Delalieux S, Sepulcre-Cantó G,  
1238 Morales F, van Aardt JAN, Sagardoy R, Coppin P, Scheunders P (2008) Model inversion  
1239 for chlorophyll estimation in open canopies from hyperspectral imagery. *International*  
1240 *Journal of Remote Sensing* 29(17-18):5093–5111
- 1241 Kiala Z, Odindi J, Mutanga O, Peerbhay K (2016) Comparison of partial least squares and  
1242 support vector regressions for predicting leaf area index on a tropical grassland using  
1243 hyperspectral data. *Journal of Applied Remote Sensing* 10(3)
- 1244 Kimes DS, Nelson RF, Manry MT, Fung AK (1998) Attributes of neural networks for ex-  
1245 tracting continuous vegetation variables from optical and radar measurements. *Internation-*  
1246 *Journal of Remote Sensing* 19(14):2639–2662
- 1247 Kira O, Nguy-Robertson A, Arkebauer T, Linker R, Gitelson A (2016) Informative spec-  
1248 tral bands for remote green LAI estimation in C3 and C4 crops. *Agricultural and Forest*  
1249 *Meteorology* 218-219:243–249
- 1250 Knox N, Skidmore A, Prins H, Asner G, van der Werff H, de Boer W, van der Waal C,  
1251 de Knegt H, Kohi E, Slotow R, Grant R (2011) Dry season mapping of savanna forage  
1252 quality, using the hyperspectral carnegie airborne observatory sensor. *Remote Sensing of*  
1253 *Environment* 115(6):1478–1488
- 1254 Knyazikhin Y, Schull MA, Stenberg P, Möttus M, Rautiainen M, Yang Y, Marshak A, Car-  
1255 mona PL, Kaufmann RK, Lewis P, et al (2013) Hyperspectral remote sensing of foliar  
1256 nitrogen content. *Proceedings of the National Academy of Sciences* 110(3):E185–E192
- 1257 Koetz B, Baret F, Poilvé H, Hill J (2005) Use of coupled canopy structure dynamic and  
1258 radiative transfer models to estimate biophysical canopy characteristics. *Remote Sensing*  
1259 *of Environment* 95(1):115–124
- 1260 Kováč D, Malenovský Z, Urban O, Špunda V, Kalina J, Ač A, Kaplan V, Hanuš J (2013) Re-  
1261 sponse of green reflectance continuum removal index to the xanthophyll de-epoxidation  
1262 cycle in norway spruce needles. *Journal of experimental botany* 64(7):1817–1827
- 1263 Labate D, Ceccherini M, Cisbani A, De Cosmo V, Galeazzi C, Giunti L, Melozzi M, Pierac-  
1264 cini S, Stagi M (2009) The PRISMA payload optomechanical design, a high performance  
1265 instrument for a new hyperspectral mission. *Acta Astronautica* 65(9-10):1429–1436
- 1266 Laurent V, Verhoef W, Damm A, Schaepman M, Clevers J (2013) A Bayesian object-based  
1267 approach for estimating vegetation biophysical and biochemical variables from APEX  
1268 at-sensor radiance data. *Remote Sensing of Environment* 139:6–17
- 1269 Laurent V, Schaepman M, Verhoef W, Weyermann J, Chávez R (2014) Bayesian object-  
1270 based estimation of LAI and chlorophyll from a simulated Sentinel-2 top-of-atmosphere  
1271 radiance image. *Remote Sensing of Environment* 140:318–329
- 1272 Lazaridis DC, Verbesselt J, Robinson AP (2010) Penalized regression techniques for predic-  
1273 tion: a case study for predicting tree mortality using remotely sensed vegetation indices.  
1274 *Canadian journal of forest research* 41(1):24–34
- 1275 Lazaro-Gredilla M, Titsias M, Verrelst J, Camps-Valls G (2014) Retrieval of biophysical pa-  
1276 rameters with heteroscedastic Gaussian processes. *IEEE Geoscience and Remote Sensing*  
1277 *Letters* 11(4):838–842



- 1278 Lee CM, Cable ML, Hook SJ, Green RO, Ustin SL, Mandl DJ, Middleton EM (2015) An  
1279 introduction to the nasa hyperspectral infrared imager (hyspirci) mission and preparatory  
1280 activities. *Remote Sensing of Environment* 167:6 – 19, DOI [https://doi.org/10.1016/j.rse.](https://doi.org/10.1016/j.rse.2015.06.012)  
1281 2015.06.012, special Issue on the Hyperspectral Infrared Imager (HyspIRI)
- 1282 Leonenko G, North P, Los S (2013) Statistical distances and their applications to biophysical  
1283 parameter estimation: Information measures, M-estimates, and minimum contrast meth-  
1284 ods. *Remote Sensing* 5(3):1355–1388
- 1285 Lewis P (1999) Three-dimensional plant modelling for remote sensing simulation studies  
1286 using the botanical plant modelling system. *Agronomie* 19(3-4):185–210
- 1287 Lewis P, Muller J (1990) Botanical plant modelling for remote sensing simulation studies.  
1288 In: *Geoscience and Remote Sensing Symposium, 1990. IGARSS'90. Remote Sensing*  
1289 *Science for the Nineties'.*, 10th Annual International, IEEE, pp 1739–1742
- 1290 Lewis P, Muller J (1993) The advanced radiometric ray tracer: Ararat for plant canopy  
1291 reflectance simulation. *International Archives of Photogrammetry and Remote Sensing*  
1292 29:26–26
- 1293 Li D, Cheng T, Zhou K, Zheng H, Yao X, Tian Y, Zhu Y, Cao W (2017) WREP: A wavelet-  
1294 based technique for extracting the red edge position from reflectance spectra for estimat-  
1295 ing leaf and canopy chlorophyll contents of cereal crops. *ISPRS Journal of Photogram-*  
1296 *metry and Remote Sensing* 129:103–117
- 1297 Li L, Zhang Q, Huang D (2014a) A review of imaging techniques for plant phenotyping.  
1298 *Sensors (Switzerland)* 14(11):20,078–20,111
- 1299 Li X, Liu X, Liu M, Wu L (2014b) Random forest algorithm and regional applications of  
1300 spectral inversion model for estimating canopy nitrogen concentration in rice. *Yaogan*  
1301 *Xuebao/Journal of Remote Sensing* 18(4):934–945
- 1302 Liang L, Di L, Zhang L, Deng M, Qin Z, Zhao S, Lin H (2015) Estimation of crop LAI  
1303 using hyperspectral vegetation indices and a hybrid inversion method. *Remote Sensing of*  
1304 *Environment* 165:123–134
- 1305 Liang L, Qin Z, Zhao S, Di L, Zhang C, Deng M, Lin H, Zhang L, Wang L, Liu Z (2016)  
1306 Estimating crop chlorophyll content with hyperspectral vegetation indices and the hybrid  
1307 inversion method. *International Journal of Remote Sensing* 37(13):2923–2949
- 1308 Lin H, Liang L, Zhang L, Du P (2013) Wheat leaf area index inversion with hyperspectral  
1309 remote sensing based on support vector regression algorithm. *Nongye Gongcheng Xue-*  
1310 *bao/Transactions of the Chinese Society of Agricultural Engineering* 29(11):139–146
- 1311 Liu WY, Pan J (2017) A hyperspectral assessment model for leaf chlorophyll content  
1312 of *Pinus massoniana* based on neural network. *Chinese Journal of Applied Ecology*  
1313 28(4):1128–1136
- 1314 Locherer M, Hank T, Danner M, Mauser W (2015) Retrieval of seasonal leaf area index  
1315 from simulated EnMAP data through optimized LUT-based inversion of the PROSAIL  
1316 model. *Remote Sensing* 7(8):10,321–10,346
- 1317 Luo J, Huang W, Zhao J, Zhang J, Zhao C, Ma R (2013) Detecting aphid density of winter  
1318 wheat leaf using hyperspectral measurements. *IEEE Journal of Selected Topics in Applied*  
1319 *Earth Observations and Remote Sensing* 6(2):690–698
- 1320 le Maire G, François C, Dufrene E (2004) Towards universal broad leaf chlorophyll indices  
1321 using PROSPECT simulated database and hyperspectral reflectance measurements. *Re-*  
1322 *remote Sensing of Environment* 89(1):1–28
- 1323 le Maire G, François C, Soudani K, Berveiller D, Pontailler JY, Bréda N, Genet H, Davi H,  
1324 Dufrene E (2008) Calibration and validation of hyperspectral indices for the estimation  
1325 of broadleaved forest leaf chlorophyll content, leaf mass per area, leaf area index and leaf  
1326 canopy biomass. *Remote Sensing of Environment* 112(10):3846–3864

- 1327 Malenovský Z, Ufer C, Lhotakova Z, Clevers J, Schaepman M, Albrechtova J, Cudlin P  
1328 (2006) A new hyperspectral index for chlorophyll estimation of a forest canopy: Area  
1329 under curve normalised to maximal band depth between 650-725 nm. *EARSel EPro-*  
1330 *ceedings* 5(2):161–172, cited By 25
- 1331 Malenovský Z, Homolová L, Zurita-Milla R, Lukeš P, Kaplan V, Hanuš J, Gastellu-  
1332 Etchegorry JP, Schaepman ME (2013) Retrieval of spruce leaf chlorophyll content from  
1333 airborne image data using continuum removal and radiative transfer. *Remote Sensing of*  
1334 *Environment* 131:85–102
- 1335 Malenovský Z, Turnbull JD, Lucieer A, Robinson SA (2015) Antarctic moss stress assess-  
1336 ment based on chlorophyll content and leaf density retrieved from imaging spectroscopy  
1337 data. *New Phytologist* 208(2):608–624
- 1338 Malenovský Z, Lucieer A, King D, Turnbull J, Robinson S (2017) Unmanned aircraft system  
1339 advances health mapping of fragile polar vegetation. *Methods in Ecology and Evolution*
- 1340 Marabel M, Alvarez-Taboada F (2013) Spectroscopic determination of aboveground  
1341 biomass in grasslands using spectral transformations, support vector machine and partial  
1342 least squares regression. *Sensors (Switzerland)* 13(8):10,027–10,051
- 1343 Mariotto I, Thenkabail P, Huete A, Slonecker E, Platonov A (2013) Hyperspectral versus  
1344 multispectral crop-productivity modeling and type discrimination for the HypSPiRI mis-  
1345 sion. *Remote Sensing of Environment* 139:291–305
- 1346 Marshall M, Thenkabail P (2014) Biomass modeling of four leading world crops using  
1347 hyperspectral narrowbands in support of HypSPiRI mission. *Photogrammetric Engineering*  
1348 *and Remote Sensing* 80(8):757–772
- 1349 Matthes J, Knox S, Sturtevant C, Sonnentag O, Verfaillie J, Baldocchi D (2015) Predicting  
1350 landscape-scale CO<sub>2</sub> flux at a pasture and rice paddy with long-term hyperspectral canopy  
1351 reflectance measurements. *Biogeosciences* 12(15):4577–4594
- 1352 Matthews M (2011) A current review of empirical procedures of remote sensing in  
1353 inland and near-coastal transitional waters. *International Journal of Remote Sensing*  
1354 32(21):6855–6899
- 1355 Meroni M, Colombo R, Panigada C (2004) Inversion of a radiative transfer model with  
1356 hyperspectral observations for LAI mapping in poplar plantations. *Remote Sensing of*  
1357 *Environment* 92(2):195–206
- 1358 Miller J, Hare E, Wu J (1990) Quantitative characterization of the vegetation red edge re-  
1359 flectance 1. An inverted-Gaussian reflectance model. *Remote Sensing* 11(10):1755–1773
- 1360 Miphokasap P, Honda K, Vaiphasa C, Souris M, Nagai M (2012) Estimating canopy nitrogen  
1361 concentration in sugarcane using field imaging spectroscopy. *Remote Sensing* 4(6):1651–  
1362 1670
- 1363 Mitchell JJ, Glenn NF, Sankey TT, Derryberry DR, Germino MJ (2012) Remote sensing of  
1364 sagebrush canopy nitrogen. *Remote sensing of environment* 124:217–223
- 1365 Montesano P, Rosette J, Sun G, North P, Nelson R, Dubayah R, Ranson K, Kharuk V (2015)  
1366 The uncertainty of biomass estimates from modeled ICESat-2 returns across a boreal  
1367 forest gradient. *Remote Sensing of Environment* 158:95–109
- 1368 Morton DC, Nagol J, Carabajal CC, Rosette J, Palace M, Cook BD, Vermote EF, Harding  
1369 DJ, North PR (2014) Amazon forests maintain consistent canopy structure and greenness  
1370 during the dry season. *Nature* 506(7487):221–224
- 1371 Mulder V, de Bruin S, Schaepman M, Mayr T (2011) The use of remote sensing in soil and  
1372 terrain mapping - a review. *Geoderma* 162(1-2):1–19
- 1373 Mutanga O, Kumar L (2007) Estimating and mapping grass phosphorus concentration in an  
1374 African savanna using hyperspectral image data. *International Journal of Remote Sensing*  
1375 28(21):4897–4911

- 1376 Mutanga O, Skidmore AK (2004) Narrow band vegetation indices overcome the saturation  
1377 problem in biomass estimation. *International Journal of Remote Sensing* 25(19):3999–  
1378 4014
- 1379 Mutanga O, Skidmore AK, Kumar L, Ferwerda J (2005) Estimating tropical pasture quality  
1380 at canopy level using band depth analysis with continuum removal in the visible domain.  
1381 *International Journal of Remote Sensing* 26(6):1093–1108
- 1382 Myneni R, Maggion S, Jaquinta J, Privette J, Gobron N, Pinty B, Kimes D, Verstraete M,  
1383 Williams D (1995) Optical remote sensing of vegetation: Modeling, caveats, and algo-  
1384 rithms. *Remote Sensing of Environment* 51(1):169–188
- 1385 Neinavaz E, Skidmore A, Darvishzadeh R, Groen T (2016) Retrieval of leaf area index in  
1386 different plant species using thermal hyperspectral data. *ISPRS Journal of Photogramme-  
1387 try and Remote Sensing* 119:390–401
- 1388 Neumann C, Förster M, Kleinschmit B, Itzerott S (2016) Utilizing a PLSR-Based Band-  
1389 Selection Procedure for Spectral Feature Characterization of Floristic Gradients. *IEEE  
1390 Journal of Selected Topics in Applied Earth Observations and Remote Sensing* 9(9):3982–  
1391 3996
- 1392 North P (1996) Three-dimensional forest light interaction model using a monte carlo  
1393 method. *IEEE Transactions on Geoscience and Remote Sensing* 34(4):946–956
- 1394 North P, Rosette J, Suárez J, Los S (2010) A Monte Carlo radiative transfer model of satellite  
1395 waveform LiDAR. *International Journal of Remote Sensing* 31(5):1343–1358
- 1396 Ollinger S (2011) Sources of variability in canopy reflectance and the convergent properties  
1397 of plants. *New Phytologist* 189(2):375–394
- 1398 Omari K, White H, Staenz K, King D (2013) Retrieval of forest canopy parameters by in-  
1399 version of the proflair leaf-canopy reflectance model using the lut approach. *IEEE Journal  
1400 of Selected Topics in Applied Earth Observations and Remote Sensing* 6(2):715–723
- 1401 Oppelt N, Mauser W (2004) Hyperspectral monitoring of physiological parameters of wheat  
1402 during a vegetation period using avis data. *International Journal of Remote Sensing*  
1403 25(1):145–159
- 1404 Paruelo J, Tomasel F (1997) Prediction of functional characteristics of ecosystems: a com-  
1405 parison of artificial neural networks and regression models. *Ecological Modelling* 98(2-  
1406 3):173–186
- 1407 Pasqualotto N, Delegido J, Wittenberghe SV, Verrelst J, Rivera JP, Moreno J (2018) Retrieval  
1408 of canopy water content of different crop types with two new hyperspectral indices: Wa-  
1409 ter absorption area index and depth water index. *International Journal of Applied Earth  
1410 Observation and Geoinformation* 67:69 – 78
- 1411 Peng Y, Huang H, Wang W, Wu J, Wang X (2011) Rapid detection of chlorophyll content  
1412 in corn leaves by using least squares-support vector machines and hyperspectral images.  
1413 *Jiangsu Daxue Xuebao (Ziran Kexue Ban)/Journal of Jiangsu University (Natural Science  
1414 Edition)* 32(2):125–128+174
- 1415 Penuelas J, Gamon JA, Fredeen AL, Merino J, Field CB (1994) Reflectance indices associ-  
1416 ated with physiological changes in nitrogen- and water-limited sunflower leaves. *Remote  
1417 Sensing of Environment* 48(2):135–146
- 1418 Pham T, Yoshino K, Bui D (2017) Biomass estimation of *Sonneratia caseolaris* (L.) Engler  
1419 at a coastal area of Hai Phong city (Vietnam) using ALOS-2 PALSAR imagery and GIS-  
1420 based multi-layer perceptron neural networks. *GIScience and Remote Sensing* 54(3):329–  
1421 353
- 1422 Pinty B, Gobron N, Widlowski JL, Gerstl S, Verstraete M, Antunes M, Bacour C, Gascon  
1423 F, Gastellu JP, Goel N, Jacquemoud S, North P, Qin W, Thompson R (2001) Radiation  
1424 transfer model intercomparison (RAMI) exercise. *Journal of Geophysical Research D:  
1425 Atmospheres* 106(D11):11,937–11,956

- 1426 Pinty B, Widlowski JL, Taberner M, Gobron N, Verstraete M, Disney M, Gascon F, Gastellu  
1427 JP, Jiang L, Kuusk A, Lewis P, Li X, Ni-Meister W, Nilson T, North P, Qin W, Su L, Tang  
1428 S, Thompson R, Verhoef W, Wang H, Wang J, Yan G, Zang H (2004) Radiation Trans-  
1429 fer Model Intercomparison (RAMI) exercise: Results from the second phase. *Journal of*  
1430 *Geophysical Research D: Atmospheres* 109(6):D06,210 1–19
- 1431 Pôças I, Gonçalves J, Costa P, Gonçalves I, Pereira L, Cunha M (2017) Hyperspectral-  
1432 based predictive modelling of grapevine water status in the Portuguese Douro wine region.  
1433 *International Journal of Applied Earth Observation and Geoinformation* 58:177–190
- 1434 Preidl S, Doktor D (2011) Comparison of radiative transfer model inversions to estimate  
1435 vegetation physiological status based on hyperspectral data
- 1436 Pu R, Gong P, Biging GS, Larrieu MR (2003) Extraction of red edge optical parameters from  
1437 Hyperion data for estimation of forest leaf area index. *IEEE Transactions on Geoscience*  
1438 *and Remote Sensing* 41(4):916–921
- 1439 Pullanagari R, Kereszturi G, Yule I (2016) Mapping of macro and micro nutrients of mixed  
1440 pastures using airborne AisaFENIX hyperspectral imagery. *ISPRS Journal of Photogram-*  
1441 *metry and Remote Sensing* 117:1–10
- 1442 Ramoelo A, Skidmore AK, Schlerf M, Mathieu R, Heitkönig IM (2011) Water-removed  
1443 spectra increase the retrieval accuracy when estimating savanna grass nitrogen and phos-  
1444 phorus concentrations. *ISPRS journal of photogrammetry and remote sensing* 66(4):408–  
1445 417
- 1446 Rasmussen CE, Williams CKI (2006) *Gaussian Processes for Machine Learning*. The MIT  
1447 Press, New York
- 1448 Rivard B, Feng J, Gallie A, Sanchez-Azofeifa A (2008) Continuous wavelets for the im-  
1449 proved use of spectral libraries and hyperspectral data. *Remote Sensing of Environment*  
1450 112(6):2850–2862
- 1451 Rivera J, Verrelst J, Leonenko G, Moreno J (2013) Multiple Cost Functions and Regular-  
1452 ization Options for Improved Retrieval of Leaf Chlorophyll Content and LAI through  
1453 Inversion of the PROSAIL Model. *Remote Sensing* 5(7):3280–3304
- 1454 Rivera J, Verrelst J, Delegido J, Veroustraete F, Moreno J (2014) On the semi-automatic  
1455 retrieval of biophysical parameters based on spectral index optimization. *Remote Sensing*  
1456 6(6):4924–4951
- 1457 Rivera JP, Verrelst J, Gómez-Dans J, Muñoz Marí J, Moreno J, Camps-Valls G (2015) An  
1458 emulator toolbox to approximate radiative transfer models with statistical learning. *Re-*  
1459 *remote Sensing* 7(7):9347
- 1460 Rivera Caicedo J, Verrelst J, Muñoz-Marí J, Moreno J, Camps-Valls G (2014) Toward a  
1461 semiautomatic machine learning retrieval of biophysical parameters. *IEEE Journal of Se-*  
1462 *lected Topics in Applied Earth Observations and Remote Sensing* 7(4):1249–1259
- 1463 Rivera-Caicedo JP, Verrelst J, Muñoz-Marí J, Camps-Valls G, Moreno J (2017) Hyperspec-  
1464 tral dimensionality reduction for biophysical variable statistical retrieval. *ISPRS Journal*  
1465 *of Photogrammetry and Remote Sensing* 132:88–101
- 1466 Roelofsen HD, Kooistra L, van Bodegom PM, Verrelst J, Krol J, Witte JPM (2014) Map-  
1467 ping a priori defined plant associations using remotely sensed vegetation characteristics.  
1468 *Remote sensing of environment* 140:639–651
- 1469 Roth K, Roberts D, Dennison P, Alonzo M, Peterson S, Beland M (2015) Differentiating  
1470 plant species within and across diverse ecosystems with imaging spectroscopy. *Remote*  
1471 *Sensing of Environment* 167:135–151
- 1472 Saich P, Lewis P, Disney M, Thackrah G (2002) Comparison of Hymap/E-SAR data with  
1473 models for optical reflectance and microwave scattering from vegetation canopies. In: *Re-*  
1474 *trieval of Bio-and Geo-Physical Parameters from SAR Data for Land Applications*, vol  
1475 475, pp 75–80

- 1476 Sanches I, Souza Filho C, Kokaly R (2014) Spectroscopic remote sensing of plant stress at  
1477 leaf and canopy levels using the chlorophyll 680nm absorption feature with continuum  
1478 removal. *ISPRS Journal of Photogrammetry and Remote Sensing* 97:111–122
- 1479 Scafutto R, de Souza Filho C, Rivard B (2016) Characterization of mineral substrates im-  
1480 pregnated with crude oils using proximal infrared hyperspectral imaging. *Remote Sensing*  
1481 *of Environment* 179:116–130
- 1482 Schlerf M, Atzberger C (2006) Inversion of a forest reflectance model to estimate structural  
1483 canopy variables from hyperspectral remote sensing data. *Remote Sensing of Environ-*  
1484 *ment* 100(3):281–294
- 1485 Schlerf M, Atzberger C, Hill J (2005) Remote sensing of forest biophysical variables using  
1486 HyMap imaging spectrometer data. *Remote Sensing of Environment* 95(2):177–194
- 1487 Schlerf M, Atzberger C, Hill J, Buddenbaum H, Werner W, Schüler G (2010) Retrieval  
1488 of chlorophyll and nitrogen in Norway spruce (*Picea abies* L. Karst.) using imaging  
1489 spectroscopy. *International Journal of Applied Earth Observation and Geoinformation*  
1490 12(1):17–26
- 1491 Shiklomanov A, Dietze M, Viskari T, Townsend P, Serbin S (2016) Quantifying the in-  
1492 fluences of spectral resolution on uncertainty in leaf trait estimates through a Bayesian  
1493 approach to RTM inversion. *Remote Sensing of Environment* 183:226–238
- 1494 Sims DA, Gamon JA (2002) Relationships between leaf pigment content and spectral re-  
1495 flectance across a wide range of species, leaf structures and developmental stages. *Remote*  
1496 *Sensing of Environment* 81(2-3):337–354
- 1497 Stimson HC, Breshears DD, Ustin SL, Kefauver SC (2005) Spectral sensing of foliar water  
1498 conditions in two co-occurring conifer species: *Pinus edulis* and *Juniperus monosperma*.  
1499 *Remote Sensing of Environment* 96(1):108–118
- 1500 Suykens J, Vandewalle J (1999) Least squares support vector machine classifiers. *Neural*  
1501 *Processing Letters* 9(3):293–300
- 1502 Thenkabail P, Smith R, De Pauw E (2000) Hyperspectral vegetation indices and their  
1503 relationships with agricultural crop characteristics. *Remote Sensing of Environment*  
1504 71(2):158–182
- 1505 Tian Y, Yao X, Yang J, Cao W, Zhu Y (2011) Extracting red edge position parameters  
1506 from ground- and space-based hyperspectral data for estimation of canopy leaf nitrogen  
1507 concentration in rice. *Plant Production Science* 14(3):270–281
- 1508 Tibshirani R (1996) Regression shrinkage and selection via the lasso. *Journal of the Royal*  
1509 *Statistical Society Series B (Methodological)* pp 267–288
- 1510 van der Tol C, Rossini M, Cogliati S, Verhoef W, Colombo R, Rascher U, Mohammed G  
1511 (2016) A model and measurement comparison of diurnal cycles of sun-induced chloro-  
1512 phyll fluorescence of crops. *Remote Sensing of Environment* 186:663–677
- 1513 Tuia D, Verrelst J, Alonso L, Pérez-Cruz F, Camps-Valls G (2011) Multioutput support  
1514 vector regression for remote sensing biophysical parameter estimation. *IEEE Geoscience*  
1515 *and Remote Sensing Letters* 8(4):804–808
- 1516 Tuia D, Volpi M, Verrelst J, Camps-Valls G (2018) Advances in kernel machines for image  
1517 classification and biophysical parameter retrieval. In: *Mathematical Models for Remote*  
1518 *Sensing Image Processing*, Springer, pp 399–441
- 1519 Uno Y, Prasher S, Lacroix R, Goel P, Karimi Y, Viau A, Patel R (2005) Artificial neural  
1520 networks to predict corn yield from compact airborne spectrographic imager data. *Com-*  
1521 *puters and Electronics in Agriculture* 47(2):149–161
- 1522 Vaglio Laurin G, Cheung-Wai Chan J, Chen Q, Lindsell J, Coomes D, Guerriero L, Del Frate  
1523 F, Miglietta F, Valentini R (2014) Biodiversity mapping in a tropical West African forest  
1524 with airborne hyperspectral data. *PLoS ONE* 9(6)

- 1525 Van Der Tol C, Verhoef W, Timmermans J, Verhoef A, Su Z (2009) An integrated model  
1526 of soil-canopy spectral radiances, photosynthesis, fluorescence, temperature and energy  
1527 balance. *Biogeosciences* 6(12):3109–3129
- 1528 Van Der Tol C, Berry J, Campbell P, Rascher U (2014) Models of fluorescence and photosyn-  
1529 thesis for interpreting measurements of solar-induced chlorophyll fluorescence. *Journal of*  
1530 *Geophysical Research: Biogeosciences* 119:2312–2327
- 1531 Vapnik V, Golowich S, Smola A (1997) Support vector method for function approximation,  
1532 regression estimation, and signal processing. *Advances in Neural Information Processing*  
1533 *Systems* 9:281–287
- 1534 Verhoef W (1984a) Light scattering by leaf layers with application to canopy reflectance  
1535 modeling: The SAIL model. *Remote Sensing of Environment* 16(2):125–141
- 1536 Verhoef W (1984b) Light scattering by leaf layers with application to canopy reflectance  
1537 modeling: The SAIL model. *Remote Sensing of Environment* 16(2):125–141
- 1538 Verhoef W (1985) Earth observation modeling based on layer scattering matrices. *Remote*  
1539 *sensing of environment* 17(2):165–178
- 1540 Verrelst J, Schaepman M, Koetz B, Kneubuhler M (2008) Angular sensitivity analysis of  
1541 vegetation indices derived from CHRIS/PROBA data. *Remote Sensing of Environment*  
1542 112(5):2341–2353
- 1543 Verrelst J, Schaepman ME, Malenovský Z, Clevers JGPW (2010) Effects of woody elements  
1544 on simulated canopy reflectance: Implications for forest chlorophyll content retrieval. *Re-*  
1545 *remote Sensing of Environment* 114(3):647–656
- 1546 Verrelst J, Alonso L, Camps-Valls G, Delegido J, Moreno J (2012a) Retrieval of vegetation  
1547 biophysical parameters using Gaussian process techniques. *IEEE Transactions on Geo-*  
1548 *science and Remote Sensing* 50(5 PART 2):1832–1843
- 1549 Verrelst J, Alonso L, Camps-Valls G, Delegido J, Moreno J (2012b) Retrieval of vegetation  
1550 biophysical parameters using Gaussian process techniques. *IEEE Transactions on Geo-*  
1551 *science and Remote Sensing* 50(5 PART 2):1832–1843
- 1552 Verrelst J, Romijn E, Kooistra L (2012c) Mapping vegetation density in a heteroge-  
1553 neous river floodplain ecosystem using pointable CHRIS/PROBA data. *Remote Sensing*  
1554 4(9):2866–2889
- 1555 Verrelst J, Alonso L, Rivera Caicedo J, Moreno J, Camps-Valls G (2013a) Gaussian process  
1556 retrieval of chlorophyll content from imaging spectroscopy data. *IEEE Journal of Selected*  
1557 *Topics in Applied Earth Observations and Remote Sensing* 6(2):867–874
- 1558 Verrelst J, Rivera J, Moreno J, Camps-Valls G (2013b) Gaussian processes uncertainty esti-  
1559 mates in experimental Sentinel-2 LAI and leaf chlorophyll content retrieval. *ISPRS Jour-*  
1560 *nal of Photogrammetry and Remote Sensing* 86:157–167
- 1561 Verrelst J, Rivera J, Leonenko G, Alonso L, Moreno J (2014) Optimizing LUT-Based RTM  
1562 Inversion for Semiautomatic Mapping of Crop Biophysical Parameters from Sentinel-  
1563 2 and -3 Data: Role of Cost Functions. *IEEE Transactions on Geoscience and Remote*  
1564 *Sensing* 52(1):257–269
- 1565 Verrelst J, Camps-Valls G, Muñoz Marí J, Rivera J, Veroustraete F, Clevers J, Moreno J  
1566 (2015) Optical remote sensing and the retrieval of terrestrial vegetation bio-geophysical  
1567 properties - A review. *ISPRS Journal of Photogrammetry and Remote Sensing* (108):273–  
1568 290
- 1569 Verrelst J, Dethier S, Rivera JP, Munoz-Mari J, Camps-Valls G, Moreno J (2016a) Active  
1570 learning methods for efficient hybrid biophysical variable retrieval. *IEEE Geoscience and*  
1571 *Remote Sensing Letters* 13(7):1012–1016
- 1572 Verrelst J, Rivera JP, Gitelson A, Delegido J, Moreno J, Camps-Valls G (2016b) Spectral  
1573 band selection for vegetation properties retrieval using Gaussian processes regression.  
1574 *International Journal of Applied Earth Observation and Geoinformation* 52:554–567

- 1575 Verrelst J, Sabater N, Rivera JP, Muñoz Marí J, Vicent J, Camps-Valls G, Moreno J (2016c)  
1576 Emulation of leaf, canopy and atmosphere radiative transfer models for fast global sensi-  
1577 tivity analysis. *Remote Sensing* 8(8):673
- 1578 Verrelst J, Rivera Caicedo J, Muñoz Marí J, Camps-Valls G, Moreno J (2017) SCOPE-based  
1579 emulators for fast generation of synthetic canopy reflectance and sun-induced fluores-  
1580 cence Spectra. *Remote Sensing* 9(9)
- 1581 Vilfan N, van der Tol C, Muller O, Rascher U, W V (2016) Fluspect-B: A model for leaf fluo-  
1582 rescence, reflectance and transmittance spectra. *Remote Sensing of Environment* 186:596  
1583 – 615
- 1584 Vohland M, Mader S, Dorigo W (2010) Applying different inversion techniques to retrieve  
1585 stand variables of summer barley with PROSPECT + SAIL. *International Journal of Ap-  
1586 plied Earth Observation and Geoinformation* 12(2):71–80
- 1587 Wang B, Chen J, Ju W, Qiu F, Zhang Q, Fang M, Chen F (2017a) Limited effects of water  
1588 absorption on reducing the accuracy of leaf nitrogen estimation. *Remote Sensing* 9(3)
- 1589 Wang F, Huang J, Lou Z (2011) A comparison of three methods for estimating leaf area  
1590 index of paddy rice from optimal hyperspectral bands. *Precision Agriculture* 12(3):439–  
1591 447
- 1592 Wang F, Huang J, Wang Y, Liu Z, Peng D, Cao F (2013) Monitoring nitrogen concentration  
1593 of oilseed rape from hyperspectral data using radial basis function. *International Journal  
1594 of Digital Earth* 6(6):550–562
- 1595 Wang J, Wang T, Skidmore A, Shi T, Wu G (2015) Evaluating different methods for grass  
1596 nutrient estimation from canopy hyperspectral reflectance. *Remote Sensing* 7(5):5901–  
1597 5917
- 1598 Wang J, Shen C, Liu N, Jin X, Fan X, Dong C, Xu Y (2017b) Non-Destructive evaluation  
1599 of the leaf nitrogen concentration by In-Field visible/Near-Infrared spectroscopy in pear  
1600 orchards. *Sensors (Switzerland)* 17(3)
- 1601 Widlowski JL, Taberner M, Pinty B, Bruniquel-Pinel V, Disney M, Fernandes R, Gastellu-  
1602 Etchegorry JP, Gobron N, Kuusk A, Lavergne T, Leblanc S, Lewis P, Martin E, Mättus  
1603 M, North P, Qin W, Robustelli M, Rochdi N, Ruiloba R, Soler C, Thompson R, Verhoef  
1604 W, Verstraete M, Xie D (2007) Third Radiation Transfer Model Intercomparison (RAMI)  
1605 exercise: Documenting progress in canopy reflectance models. *Journal of Geophysical  
1606 Research D: Atmospheres* 112(9)
- 1607 Widlowski JL, Pinty B, Clerici M, Dai Y, De Kauwe M, De Ridder K, Kallel A, Kobayashi  
1608 H, Lavergne T, Ni-Meister W, Olchev A, Quaife T, Wang S, Yang W, Yang Y, Yuan H  
1609 (2011) RAMI4PILPS: An intercomparison of formulations for the partitioning of solar  
1610 radiation in land surface models. *Journal of Geophysical Research G: Biogeosciences*  
1611 116(2)
- 1612 Widlowski JL, Mio C, Disney M, Adams J, Andredakis I, Atzberger C, Brennan J, Busetto  
1613 L, Chelle M, Ceccherini G, et al (2015) The fourth phase of the radiative transfer model  
1614 intercomparison (RAMI) exercise: Actual canopy scenarios and conformity testing. *Re-  
1615 mote Sensing of Environment* 169:418–437
- 1616 Wold S, Esbensen K, Geladi P (1987) Principal component analysis. *Chemometrics and  
1617 Intelligent Laboratory Systems* 2(1-3):37–52
- 1618 Xue J, Su B (2017) Significant remote sensing vegetation indices: A review of developments  
1619 and applications. *Journal of Sensors* 2017
- 1620 Yang P, Verhoef W, van der Tol C (2017) The mSCOPE model: A simple adaptation to  
1621 the SCOPE model to describe reflectance, fluorescence and photosynthesis of vertically  
1622 heterogeneous canopies. *Remote Sensing of Environment* 201:1–11
- 1623 Yang X, Huang J, Wu Y, Wang J, Wang P, Wang X, Huete A (2011) Estimating biophysical  
1624 parameters of rice with remote sensing data using support vector machines. *Science China*

- 1625 Life Sciences 54(3):272–281
- 1626 Yao X, Huang Y, Shang G, Zhou C, Cheng T, Tian Y, Cao W, Zhu Y (2015) Evaluation of six  
1627 algorithms to monitor wheat leaf nitrogen concentration. *Remote Sensing* 7(11):14,939–  
1628 14,966
- 1629 Ye X, Sakai K, Manago M, Asada SI, Sasao A (2007) Prediction of citrus yield from airborne  
1630 hyperspectral imagery. *Precision Agriculture* 8(3):111–125
- 1631 Yi Q, Jiapaer G, Chen J, Bao A, Wang F (2014) Different units of measurement of  
1632 carotenoids estimation in cotton using hyperspectral indices and partial least square re-  
1633 gression. *ISPRS Journal of Photogrammetry and Remote Sensing* 91:72–84
- 1634 Yin T, Lauret N, Gastellu-Etchegorry JP (2016) Simulation of satellite, airborne and terres-  
1635 trial LIDAR with DART (II): ALS and TLS multi-pulse acquisitions, photon counting,  
1636 and solar noise. *Remote Sensing of Environment* 184:454–468
- 1637 Yue J, Yang G, Li C, Li Z, Wang Y, Feng H, Xu B (2017) Estimation of winter wheat above-  
1638 ground biomass using unmanned aerial vehicle-based snapshot hyperspectral sensor and  
1639 crop height improved models. *Remote Sensing* 9(7)
- 1640 Zandler H, Brenning A, Samimi C (2015) Quantifying dwarf shrub biomass in an arid en-  
1641 vironment: Comparing empirical methods in a high dimensional setting. *Remote Sensing*  
1642 of Environment 158:140–155
- 1643 Zarco-Tejada P, Miller J, Noland T, Mohammed G, Sampson P (2001) Scaling-up and model  
1644 inversion methods with narrowband optical indices for chlorophyll content estimation in  
1645 closed forest canopies with hyperspectral data. *IEEE Transactions on Geoscience and*  
1646 *Remote Sensing* 39(7):1491–1507
- 1647 Zarco-Tejada P, Miller J, Mohammed G, Noland T, Sampson P (2002) Vegetation stress  
1648 detection through chlorophyll+ estimation and fluorescence effects on hyperspectral im-  
1649 agery. *Journal of environmental quality* 31(5):1433–1441
- 1650 Zhang S, Wang Q (2015) Inverse retrieval of chlorophyll from reflected spectra for assimilating  
1651 branches of drought-tolerant *Tamarix ramosissima*. *IEEE Journal of Selected Topics*  
1652 *in Applied Earth Observations and Remote Sensing* 8(4):1498–1505
- 1653 Zhang Y, Chen J, Miller J, Noland T (2008) Leaf chlorophyll content retrieval from airborne  
1654 hyperspectral remote sensing imagery. *Remote Sensing of Environment* 112(7):3234–  
1655 3247